iScience

CellPress
OPEN ACCESS

Article

Mechanistic impact of oligomer poisoning by dominant-negative CARD11 variants

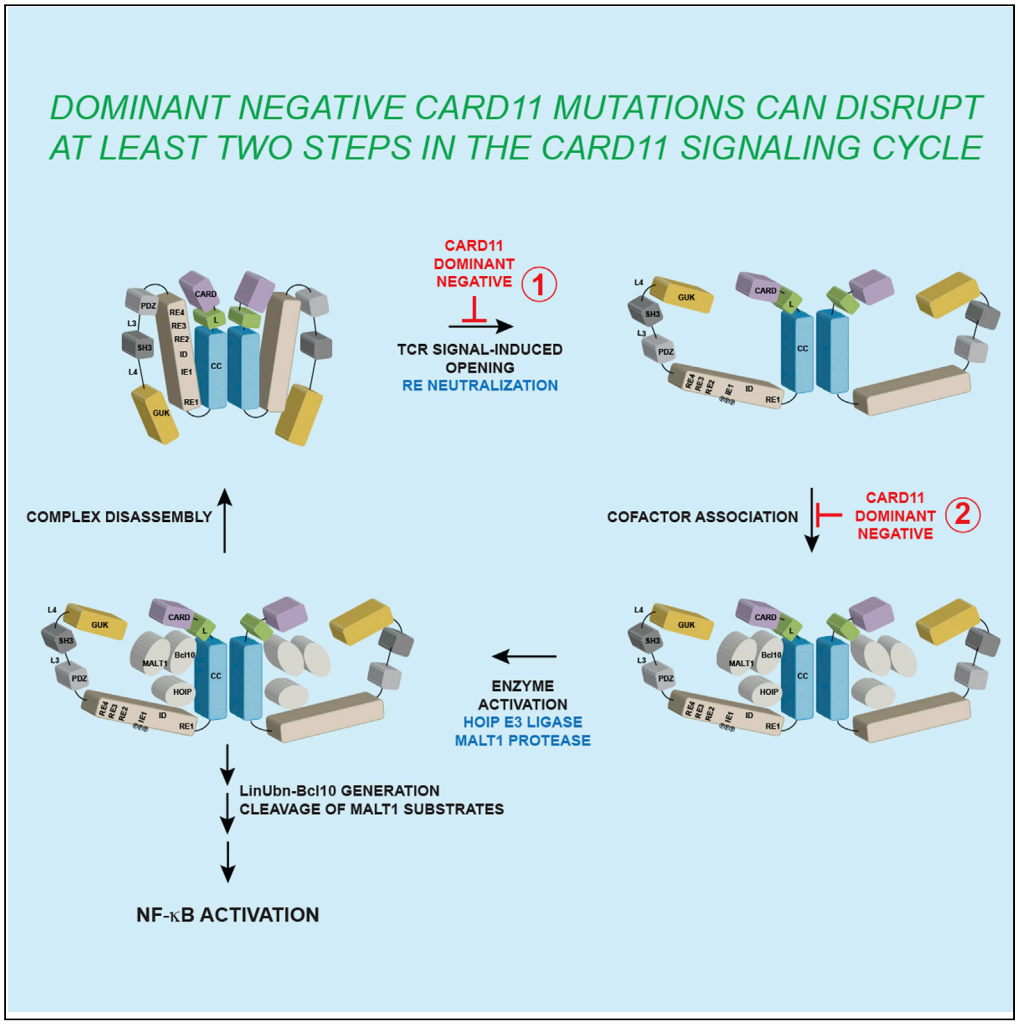

Jacquelyn R. Bedsaul, Neha Shah, Shelby M. Hutcherson, Joel L. Pomerantz

joel.pomerantz@jhmi.edu

Highlights

Dominant-negative CARD11 mutants can disrupt the TCR-induced opening of CARD11 oligomers

Dominant-negative CARD11 mutants can also impair cofactor association with CARD11

CARD11 CARD and LATCH domain residues are required for the Opening Step

CARD domain residues coordinate at least two steps in the CARD11 signaling cycle

Bedsaul et al., iScience 25, 103810
February 18, 2022
https://doi.org/10.1016/j.isci.2022.103810

iScience

CellPress
OPEN ACCESS

Article

Mechanistic impact of oligomer poisoning by dominant-negative CARD11 variants

Jacquelyn R. Bedsaul,[1] Neha Shah,[1] Shelby M. Hutcherson,[1] and Joel L. Pomerantz[1,2,*]

SUMMARY

The CARD11 scaffold controls antigen receptor signaling to NF-κB, JNK, and mTOR. Three classes of germline mutations in CARD11 cause Primary Immunodeficiency, including homozygous loss-of-function (LOF) mutations in CARD11 deficiency, heterozygous gain-of-function (GOF) mutations in BENTA disease, and heterozygous dominant-negative LOF mutations in CADINS. Here, we characterize LOF CARD11 mutants with a range of dominant-negative activities to identify the mechanistic properties that cause these variants to exert dominant effects when heterozygous. We find that strong dominant negatives can poison signaling from mixed wild-type:mutant oligomers at two steps in the CARD11 signaling cycle, at the Opening Step and at the Cofactor Association Step. Our findings provide evidence that CARD11 oligomer subunits cooperate in at least two steps during antigen receptor signaling and reveal how different LOF mutations in the same oligomeric signaling hub may cause disease with different inheritance patterns.

INTRODUCTION

The appropriate response of B and T lymphocytes to a pathogen depends on antigen receptor signaling pathways that orchestrate broad changes in gene expression required for lymphocyte activation and differentiation. Germline mutations in genes encoding components of the antigen receptor signaling pathways frequently result in Primary Immunodeficiency syndromes, leading to impaired immunity and recurrent infections in affected individuals (Notarangelo et al., 2020; Tangye et al., 2020). However, in many cases, the precise molecular mechanisms by which a given inherited mutation mechanistically perturbs signaling and leads to the patient phenotype are not well understood.

CARD11 is a multidomain signaling scaffold that functions as a central signaling hub downstream of antigen receptor engagement that governs the antigen-induced activation of branched pathways that induce NF-κB, mTOR, and JNK (Bedsaul et al., 2018; Lork et al., 2019; Thys et al., 2018). CARD11 scaffold activity is inducible and tightly controlled (Lamason et al., 2010a; Pedersen et al., 2016). In resting B and T lymphocytes, CARD11 is kept in a closed, inactive state owing to the cooperative autoinhibitory action of four repressive elements (REs) within the Inhibitory Domain that function with redundancy to prevent the association of cofactors, in part through intramolecular interactions with other CARD11 domains (Jattani et al., 2016a; 2016b). Upon antigen receptor triggering, CARD11 activity is induced through several defined steps in the CARD11 signaling cycle (Wang et al., 2019). First, in a poorly understood Opening Step, the inhibitory REs are neutralized and CARD11 converts to an open, active state in which surfaces of CARD and Coiled-coil domains become exposed and available for binding proteins *in trans*. Second, in the Cofactor Association Step, a variety of signaling cofactors are recruited to CARD11, including the adapter Bcl10, the protease MALT1, the E3 ubiquitin ligase HOIP, and several others. MALT1 is recruited to CARD11 through its interaction with Bcl10 and performs essential functions in signaling both as a scaffold, for example for the recruitment of the E3 ubiquitin ligase TRAF6, and as a protease (Juilland and Thome, 2018; O'Neill et al., 2021; Schlauderer et al., 2018; Sun et al., 2004). In the third distinguishable Enzyme Activation Step (Wang et al., 2019), the catalytic activities of HOIP and MALT1 are activated, leading to the HOIP-mediated conjugation of Bcl10 with linear ubiquitin chains to form $LinUb_n$-Bcl10 and the MALT1-mediated cleavage of several key substrates. $LinUb_n$-Bc10 associates with the IKK complex and contributes to optimal IKK kinase activation in the pathway leading to NF-κB induction (Yang et al., 2016). The cleavage of A20, CYLD, HOIL-1, Bcl10, and RelB by MALT1 also modulates the extent and duration of NF-κB activation downstream of CARD11 (Juilland and Thome, 2018). In the fourth Complex

[1]Department of Biological Chemistry and Institute for Cell Engineering, The Johns Hopkins University School of Medicine, Baltimore, MD 21205, USA

[2]Lead contact

*Correspondence: joel.pomerantz@jhmi.edu

https://doi.org/10.1016/j.isci.2022.103810

Disassembly Step of the CARD11 signaling cycle, signaling cofactors disassociate from CARD11 and CARD11 reverts to the closed, inactive resting state (Bedsaul et al., 2018). CARD11 has also been shown to promote Bcl10 polymerization into filaments *in vitro*, which can amplify the proteolytic activity of associated MALT1 (David et al., 2018; Qiao et al., 2013; Schlauderer et al., 2018). The formation of Bcl10 filaments likely occurs subsequent to the Cofactor Association Step in the CARD11 signaling cycle. The different steps in the CARD11 signaling cycle have been distinguished by the selective effects of gain-of-function (GOF) and loss-of-function (LOF) CARD11 mutations. For example, the Opening Step is prevented by several LOF mutations within Inducibility Element 1 (IE1) in the Inhibitory Domain at residues that do not participate directly in CARD11:cofactor protein–protein interactions but are required for the process by which upstream signaling makes the CARD and Coiled-coil accessible for cofactor binding (Matsumoto et al., 2005; McCully and Pomerantz, 2008; Shinohara et al., 2007; Sommer et al., 2005; Wang et al., 2019). The Opening Step is bypassed by the combined mutation of two or more REs and by GOF mutations in the CARD, LATCH, and Coiled-coil domains that prevent the intramolecular binding of REs (Chan et al., 2013; Jattani et al., 2016a; 2016b; Lamason et al., 2010b) but also do not participate directly in CARD11:cofactor interfaces. The Enzyme Activation Step is distinguishable from the Cofactor Association Step by the LOF mutation of several IE1 residues that prevent the activation of HOIP E3 and MALT1 protease activities in the context of a constitutively open CARD11 variant that constitutively binds cofactors due to the simultaneous mutation and constitutive neutralization of all four REs (Wang et al., 2019).

In both resting and activated states, CARD11 exists in the cytoplasm as an oligomer of undetermined stoichiometry through interactions mediated by the Coiled-coil domain (Tanner et al., 2007). How the different CARD11 subunits in the assembled oligomer cooperate or influence each other's activity during the CARD11 signaling cycle is presently unclear.

At least three forms of Primary Immunodeficiency are due to germline mutations in the gene encoding CARD11 (Lu et al., 2019; Turvey et al., 2014). These three diseases, caused by different classes of CARD11 mutations, are referred to as CARD11 deficiency, B cell Expansion with NF-κB and T cell Anergy (BENTA), and CARD11-associated Atopy with Dominant Interference of NF-κB Signaling (CADINS). CARD11 deficiency is caused by homozygous LOF mutations in CARD11 and is associated with severe *Pneumocystis jirovecii* infections, hypogammaglobulinemia, deficits in mature or differentiated B and T cells, and defective B and T cell activation *in vitro* (Greil et al., 2013; Lu et al., 2021; Stepensky et al., 2013). BENTA disease is caused by heterozygous GOF CARD11 mutations (Snow et al., 2012). Patients with BENTA experience recurrent ear, sinopulmonary and viral infections (*Molluscum contagiosum*, BK virus, and Epstein–Barr virus) and exhibit a profound expansion in the number of B cells, a skewing of B cells toward transitional states, unresponsiveness of T cells to antigen, and a poor antibody response to pneumococcal and meningococcal capsular polysaccharides (Arjunaraja et al., 2017, 2018; Brohl et al., 2014; Buchbinder et al., 2015; Snow et al., 2012). CADINS is caused by heterozygous LOF CARD11 mutations that act as strong dominant-negative alleles (Dadi et al., 2018; Dorjbal et al., 2019; Izadi et al., 2021; Ma et al., 2017). Affected individuals frequently experience severe atopic dermatitis, recurrent pneumonia and other upper respiratory tract infections, skin infections, asthma, and allergies to food and environmental antigens with varying severities. WhileCADINS patient B cells exhibit mild defects in antigen-induced activation, patient T cells display reduced activation and proliferation *in vitro*, consistent with a poor T cell response to prior antigen exposure. Patients also display elevated serum IgE levels but low-to-normal levels of other Ig classes (Dadi et al., 2018; Dorjbal et al., 2019; Izadi et al., 2021; Ma et al., 2017). A mouse model of CADINS recapitulates several features of the human syndrome (Hutcherson et al., 2021).

Dominant-negative LOF CARD11 variants, including those associated with CADINS, must be mechanistically distinct from other LOF mutations, such as those associated with CARD11 deficiency, because they possess the unique ability to perturb signaling from a co-expressed wild-type CARD11 protein. In this report, we investigate the mechanistic basis for dominant-negative CARD11 activity and discover that at least two steps in the CARD11 signaling cycle can be targeted by this class of CARD11 mutations.

RESULTS

Theoretical poisoning of CARD11 oligomers by dominant-negative mutants

We previously reported primary immunodeficiency and atopy in a family in which affected individuals were heterozygous for the CARD11 R30W mutation (Dadi et al., 2018). Our characterization of CARD11 R30W

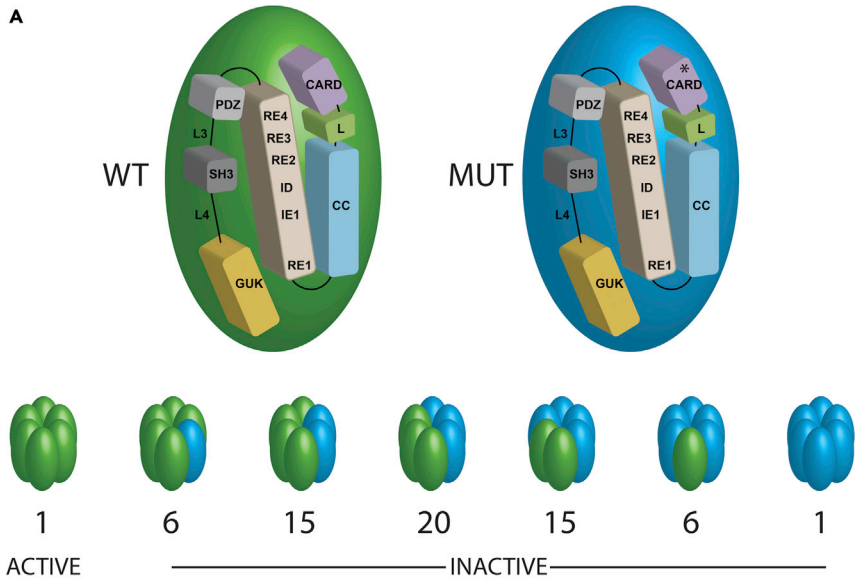

B

STOICHIOMETRY	FRACTION OF OLIGOMERS THAT ARE ACTIVE
2	1/4
3	1/8
4	1/16
5	1/32
6	1/64
7	1/128

Figure 1. Theoretical poisoning of CARD11 oligomers by dominant-negative mutants

(A) Co-expression of wild-type (green ellipsoid) and mutant (blue ellipsoid) CARD11 variants will lead to the random population of oligomers of different species containing 0 to n mutant subunits, as predicted by the binomial expansion of $(WT + MUT)^n$, where n equals the number of subunits per oligomer. The example of a symmetrical hexamer (n = 6) is depicted. The binomial coefficients predict the relative proportions of each oligomeric species in a total of 64 oligomers as follows: 1 (6WT:0MUT); 6 (5WT:1MUT); 15 (4WT:2MUT); 20 (3WT:3MUT); 15 (2WT:4MUT); 6 (1WT:5MUT); 1 (0WT:6MUT). If one mutant subunit is sufficient to poison the activity of the oligomer, then the 6WT:0MUT species will be active, while all other species will be inactive. This would result in an observed activity equivalent to that elicited by 1.56% (1/64) of all wild-type oligomers expressed at the same total amount.

(B) The fraction of oligomers that are active at a given stoichiometry of the CARD11 oligomer are depicted, calculated with the binomial expansion for n = 2 through n = 7. The active fraction is calculated with the assumptions that the WT and MUT subunits have equal propensities to assemble into oligomers and that one MUT subunit is sufficient to poison the signaling activity of an oligomer, such that only all-WT oligomers are active.

indicated a profound dominant-negative capability of this variant to reduce T cell receptor (TCR)-induced signaling from a co-expressed wild-type CARD11 protein by >95% (Dadi et al., 2018). Since CARD11 signals as an oligomer of unknown stoichiometry, we reasoned that this level of dominant-negative inhibition could be rationalized if wild-type and mutant CARD11 proteins assemble randomly into oligomers and if one mutant subunit within an oligomer is sufficient to poison the signaling capability of that oligomer. For example, if the CARD11 oligomer is a symmetrical hexamer, equivalent amounts of mutant and wild-type subunits will sort into oligomers containing 0,1, 2, 3, 4, 5, or 6 mutant subunits with predictable relative frequencies according to the binomial distribution (Figure 1A). If the presence of a single mutant subunit is sufficient to completely inactivate the CARD11 oligomer, then only 1 out of 64 hexameric oligomers will be composed of all wild-type subunits and be competent to signal; this would lead to a drop in signaling potential to a level equivalent to that elicited by 1.56% of an equally expressed wild-type protein that assembles into oligomers in the absence of the mutant. One can similarly calculate the fraction of functional oligomers that would result from the equal expression of wild-type and mutant subunits for other oligomerization stoichiometries (Figure 1B). This rationalization could help explain why a dominant-negative

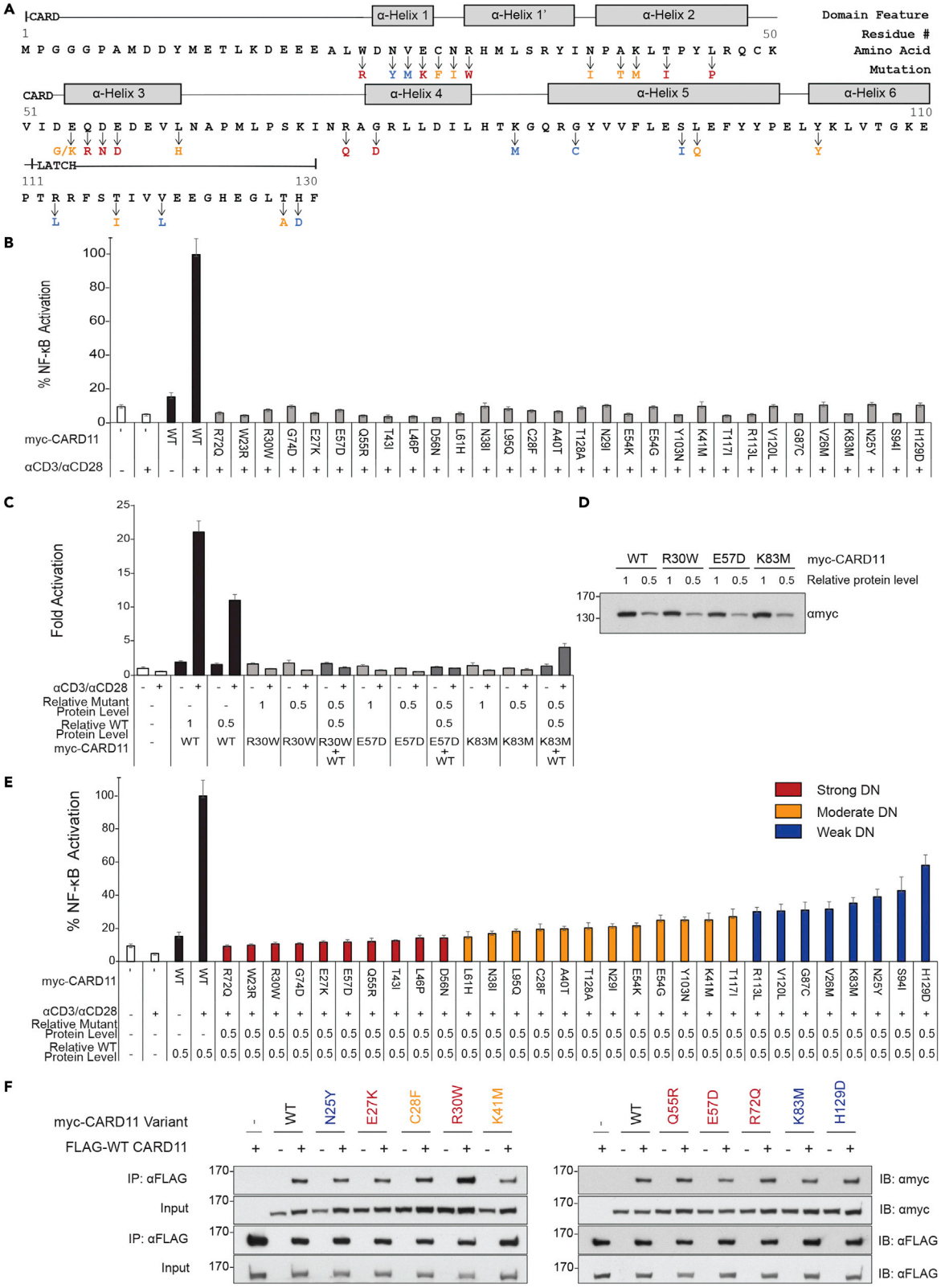
A
CARD
α-Helix 1
α-Helix 1'
α-Helix 2
Domain Feature
Residue #
Amino Acid
Mutation
CARD
α-Helix 3
α-Helix 4
α-Helix 5
α-Helix 6
LATCH
B
% NF-κB Activation
myc-CARD11
αCD3/αCD28
C
Fold Activation
αCD3/αCD28
Relative Mutant Protein Level
Relative WT Protein Level
myc-CARD11
D
WT R30W E57D K83M myc-CARD11
Relative protein level
αmyc
E
% NF-κB Activation
Strong DN
Moderate DN
Weak DN
myc-CARD11
αCD3/αCD28
Relative Mutant Protein Level
Relative WT Protein Level
F
myc-CARD11 Variant
FLAG-WT CARD11
IP: αFLAG
Input
IP: αFLAG
Input
IB: αmyc
IB: αmyc
IB: αFLAG
IB: αFLAG

Figure 2. A panel of LOF CARD11 mutants exhibits a range of dominant-negative activity

(A) The amino-terminal 130 residues of murine CARD11 are depicted with the locations of the CARD domain helices from (Li et al., 2012) and LATCH domain annotated. The mutations examined in this study are indicated and color coded for relative dominant-negative potency of strong (red), moderate (yellow), or weak (blue).

(B) NF-κB luciferase reporter activity in CARD11-deficient (CARD11-KO) Jurkat T cells in which cells were transiently transfected with myc-CARD11 variants expressed at equivalent protein levels and stimulated with anti-CD3/anti-CD28 for 4–5 h. Relative activity is depicted as a percent of the NF-κB activation achieved with wild-type (WT) CARD11 after stimulation, which corresponds to an average fold activation of 12.0. Bars and error bars indicate mean relative activity with standard deviation (SD). A two-tailed unpaired Student's *t* test with Welch's correction resulted in p values of <0.0001 for the values of all CARD11 mutants obtained under stimulated conditions as compared with that observed for WT CARD11 under stimulated conditions.

(C) NF-κB luciferase reporter activity in CARD11-KO Jurkat T cells in which cells were transiently transfected with myc-WT CARD11 (black) or myc-R30W, myc-E57D, or myc-K83M CARD11 mutants (light gray), or co-transfected with myc-tagged WT and mutants together (dark gray) at equivalent protein levels and stimulated with anti-CD3/anti-CD28 for 4 h. Bars and error bars indicate mean fold activation with SD. A two-tailed unpaired Student's *t* test with Welch's correction resulted in the following p values for the values of the CARD11 mutants in the absence and presence of co-expressed WT CARD11 obtained under stimulated conditions as compared with that observed for wild-type CARD11 at the 0.5 relative protein level under stimulated conditions: R30W, p = 0.0021; R30W + WT, p = 0.0018; E57D, p = 0.0020; E57D + WT, p = 0.0022; K83M, p = 0.0014; and K83M + WT, p = 0.0005.

(D) Equivalent protein levels of myc-tagged WT and CARD11 variants determined by transient transfection of HEK293T cells as described in the STAR methods followed by Western blotting for myc with the following concentrations of DNA used to achieve 1 and 0.5 relative protein levels of CARD11, respectively: 120 and 63 ng myc-WT, 250 and 110 ng myc-R30W, 140 and 70 ng myc-E57D, and 150 and 65 ng myc-K83M CARD11.

(E) NF-κB luciferase reporter activity in CARD11-KO Jurkat T cells in which the cells were co-transfected with myc-WT and myc-mutant CARD11 at equivalent protein levels and stimulated with anti-CD3/anti-CD28 for 4–5 h. Relative activity is depicted as a percent of the NF-κB activation achieved with WT CARD11 after stimulation, which corresponds to an average fold activation of 12.0. Bars and error bars indicate mean relative activity with SD. A two-tailed unpaired Student's t test with Welch's correction resulted in p values of $p < 0.0001$ for the values of all CARD11 mutants co-expressed with WT CARD11 obtained under stimulated conditions as compared with that observed for WT CARD11 under stimulated conditions. Dominant-negative (DN) strength is denoted by color and calculated by subtracting out the background activation of stimulated CARD11-KO cells: strong <10% activation (red), moderate 10–25% activation (yellow), and weak >25% activation (blue).

(F) A representative set of ten myc-tagged CARD11 variants or myc-WT CARD11 were transiently transfected in HEK293T cells with 200ng FLAG-WT CARD11 for co-immunoprecipitation assays. At 40–41 h, cells were lysed and co-immunoprecipitated with rabbit anti-FLAG followed by Western blotting for myc and FLAG. The following concentrations of DNA were used to achieve roughly equivalent protein expression for the FLAG-WT CARD11 co-immunoprecipitation: 200 ng FLAG-WT, 200 ng myc-WT, 325 ng myc-N25Y, 500 ng myc-E27K, 250 ng myc-C28F, 500 ng myc-R30W, 275 ng myc-K41M, 300 ng myc-Q55R, 300 ng myc-E57D, 200 ng myc-R72Q, 500 ng myc-K83M, and 200 ng myc-H129D.

CARD11 mutant could precipitously inhibit signaling and manifest immunological dysfunction in heterozygous patients. Other scenarios are also possible, such as the requirement for two mutant subunits to poison oligomer activity. Similar considerations have been useful for understanding other oligomeric proteins, including ion channels (Balannik et al., 2008; MacKinnon, 1991), and for determining the subunit stoichiometry of viral assembly components (Fang et al., 2014; Trottier and Guo, 1997).

Not all LOF CARD11 mutations are dominant-negative, as indicated by the LOF alleles inherited in CARD11 deficiency that cause disease only when homozygous. In principle, a particular LOF allele could be dominant-negative, and poison the activity of a CARD11 oligomer, if its mutation impairs one or more steps in the CARD11 signaling cycle that require the participation of all (or most) subunits in the oligomer. In contrast, LOF alleles that do not act as dominant negatives might impair a signaling step that does not require the participation of all or most oligomer subunits, which would proceed in oligomers that have one or more mutant CARD11 subunits, as in the heterozygous state, and would not proceed when all subunits are mutant, as in the homozygous state.

To investigate which steps in the CARD11 signaling cycle are susceptible to dominant-negative mutations, we studied a panel of LOF CARD11 mutants, many of which we had previously isolated as a byproduct of a screen for GOF CARD11 variants (Chan et al., 2013). Our goals were to quantitate the relative dominant-negative activity of mutants in this panel, assay which step is impacted by representative mutants in the absence and presence of co-expressed wild-type CARD11, and determine whether one or more steps are more affected by strong dominant-negative mutants than by weak dominant-negative mutants.

Our panel included the following 28 mutations: W23R, N25Y, V26M, E27K, N29I, R30W, N38I, A40T, K41M, T43I, L46P, E54K, E54G, Q55R, D56N, E57D, L61H, G74D, K83M, G87C, S94I, L95Q, Y103N, T117I, R113L, V120L, T128A, and H129D. We also analyzed C28F and R72Q, two other CARD11 mutations that have previously been identified in a screen for defective CARD11 variants (Meitlis et al., 2020). All of these mutations are located in either the CARD or LATCH domains within the N-terminal 129 residues of murine CARD11 (Figure 2A).

A panel of LOF CARD11 mutations that exhibit a range of dominant-negative activities

First, we determined the signaling potential of each mutant in TCR signaling to NF-κB, as compared to that of wild-type CARD11, in a well-established NF-κB luciferase reporter assay in Jurkat T cells in which endogenous CARD11 expression has been eliminated via lentiviral-mediated CRISPR/Cas9 genomic editing (Yang et al., 2016). These CARD11 deficient (CARD11-KO) Jurkat T cells were transiently transfected with the expression vector for each CARD11 variant along with the Igκ$_2$-IFN-LUC reporter, and the CSK-LacZ vector expressing β-galactosidase, which was used for the normalization of transfection efficiency and extract recovery (McCully and Pomerantz, 2008). We used concentrations of expression vectors that yielded comparable expression levels for each CARD11 variant (Figure S1). Transfected cells were then treated in the absence and presence of anti-CD3/anti-CD28 to trigger TCR signaling. As shown in Figure 2B, the reconstitution of CARD11-KO Jurkat T cells with wild-type murine CARD11 resulted in robust 12-fold activation of NF-κB by anti-CD3/anti-CD28 cross-linking. In contrast, each of the 30 mutants we assayed failed to rescue inducible signaling to NF-κB, verifying that each of these variants is a severe LOF CARD11 mutant that fails to propagate signaling when assembled into all-mutant CARD11 oligomers. Their relative activities in this assay as compared to wild-type CARD11 are listed in Table 1.

Next, we assessed the dominant-negative activity of each mutant using the same NF-κB luciferase reporter assay. CARD11-KO Jurkat T cells were transfected with expression vectors for wild-type CARD11, mutant CARD11, or both wild-type and mutant CARD11 variants together at concentrations that resulted in equivalent protein levels. A representative assay is depicted in Figures 2C and 2D, in which R30W, E57D, and K83M CARD11 variants were assayed. Co-expression of R30W and E57D with wild-type CARD11 eliminated anti-CD3/anti-CD28-induced signaling to NF-κB, even though the equivalent amount of wild-type CARD11 expressed alone resulted in 11-fold activation, indicating that both of these mutants had strong dominant-negative activity. In contrast, co-expression of the K83M mutant with wild-type CARD11 reduced signaling from the 11-fold observed with wild-type alone to 4.1-fold, revealing a weaker dominant-negative effect than that observed with R30W or E57D. The dominant-negative activity of all 30 LOF mutants was quantitated by the same assay. The relative activity of each mutant when co-expressed with wild-type CARD11 in TCR signaling to NF-κB is depicted in Figure 2E and listed in Table 1. Our panel of mutants exhibited a range of dominant-negative activities, from 96% inhibition of co-expressed wild-type CARD11 to only 44% inhibition. We refer to these mutants as strong, moderate, or weak dominant negatives based on the ability to inhibit co-expressed wild type by >90%, 75–90%, or <75%, respectively (Figure 2E, Table 1). All of the mutants we assayed lie outside of the Coiled-coil domain, which has been shown to mediate CARD11 oligomerization (Tanner et al., 2007). We tested ten representative strong, moderate, and weak dominant-negative mutants for the ability to associate with wild-type CARD11 in a co-immunoprecipitation assay after expression in HEK293T cells (Figure 2F). All mutants tested could robustly associate with wild-type CARD11 with similar relative efficiencies that did not correlate with relative dominant-negative activity, indicating similar propensities to assemble into oligomers.

We mapped the location of these mutations in the crystal structure of the CARD11 CARD domain (Li et al., 2012) to determine whether a particular surface of the domain was populated by mutants with similar activities. As shown in Figure S2, residues that lead to strong dominant-negative activity when mutated, shown in red, do not cluster at a single surface of the domain; rather, they are distributed over several regions of the domain surface and are located in multiple helices and loops (also see Figure 2A and Table 1). Residues that lead to moderate or weak dominant-negative activity when mutated, in yellow and blue, respectively, also do not map to a single surface and are dispersed throughout the CARD domain.

CARD and LATCH mutants disrupt the Opening Step in the CARD11 signaling cycle

Next, we analyzed the subset of ten mutants with a range of dominant-negative activities to determine the steps in the CARD11 signaling cycle that they perturbed when expressed in the absence of wild-type CARD11 and therefore operating in CARD11 oligomers composed only of mutant CARD11 subunits. We used retroviral infection to stably reconstitute CARD11-KO Jurkat T cells with either wild-type CARD11 or ten variants shown to have strong (E27K, R30W, Q55R, E57D, R72Q), moderate (C28F, K41M), or weak (N25Y, K83M, H129D) dominant-negative activity. As expected, stable reconstitution with each mutant resulted in severe defects in anti-CD3/anti-CD28-induced NF-κB activation when compared to wild-type CARD11, as assessed in the Igκ$_2$-IFN-LUC reporter assay (Figure 3A).

Table 1. Summary of the percent NF-κB activation of CARD11 mutations compared to wild-type CARD11 in the presence and absence of equivalent protein level of wild-type CARD11 following the transient transfection and NF-κB luciferase reporter assay in CARD11-deficient Jurkat T cells

CARD11 mutations	% NF-κB activation Mutant	% NF-κB activation mutant + WT	Domain	α-Helix
WT	100	100	–	–
W23R	ND	4.8	CARD	–
N25Y	5.6	35.6	CARD	α-Helix 1
V26M	5.3	27.8	CARD	α-Helix 1
E27K	0.2	6.7	CARD	α-Helix 1
C28F	1.7	14.9	CARD	–
N29I	5.1	16.6	CARD	–
R30W	2.2	5.6	CARD	α-Helix 1′
N38I	4.4	12.1	CARD	–
A40T	1.2	15.2	CARD	α-Helix 2
K41M	4.5	20.8	CARD	α-Helix 2
T43I	ND	7.7	CARD	α-Helix 2
L46P	ND	9.4	CARD	α-Helix 2
E54G	4.1	20.6	CARD	α-Helix 3
E54K	ND	17.1	CARD	α-Helix 3
Q55R	ND	7.1	CARD	α-Helix 3
D56N	ND	9.4	CARD	α-Helix 3
E57D	2.2	6.7	CARD	α-Helix 3
L61H	ND	10.0	CARD	α-Helix 3
R72Q	0.4	4.0	CARD	–
G74D	4.4	5.6	CARD	α-Helix 4
K83M	1.9	31.6	CARD	–
G87C	ND	27.2	CARD	α-Helix 5
S94I	ND	39.5	CARD	α-Helix 5
L95Q	2.9	13.7	CARD	α-Helix 5
Y103N	ND	20.8	CARD	α-Helix 6
R113L	ND	26.2	LATCH	–
T117I	ND	22.9	LATCH	–
V120L	4.5	26.6	LATCH	–
T128A	3.6	15.8	LATCH	–
H129D	5.2	55.8	LATCH	–

ND: not detected; activity was below the background percent NF-κB activation for CARD11-KO Jurkat T cells stimulated with anti-CD3/anti-CD28 cross-linking.

During the Enzyme Activation Step in the CARD11 signaling cycle, the E3 ligase activity of HOIP, the catalytic subunit of the Linear Ubiquitin Chain Assembly Complex (LUBAC), is activated and proceeds to conjugate Bcl10 with linear ubiquitin chains to form $LinUb_n$-Bcl10, a key signaling intermediate that determines the output of signaling to NF-κB (Yang et al., 2016). We measured the ability of the stably expressed CARD11 variants to support TCR-inducible $LinUb_n$-Bcl10 generation by immunoprecipitating Bcl10 under denaturing conditions from stimulated cell extracts and blotting the immunoprecipitates using antibodies specific for linear ubiquitin chains, as previously described (Yang et al., 2016). All CARD11 mutants analyzed exhibited defects in $LinUb_n$-Bcl10 generation, with no intermediate detected in the presence of the E27K, C28F, R30W, K41M, Q55R, E57D, R72Q, and K83M mutants, and some intermediate detected with N25Y and H129D (Figure 3B). We also measured the CARD11-dependent activation of MALT1 protease activity, which also occurs during the Enzyme Activation Step. We stimulated the reconstituted cells with anti-CD3/anti-CD28 cross-linking and assayed the production of cleavage products of MALT1 substrates HOIL-1 and

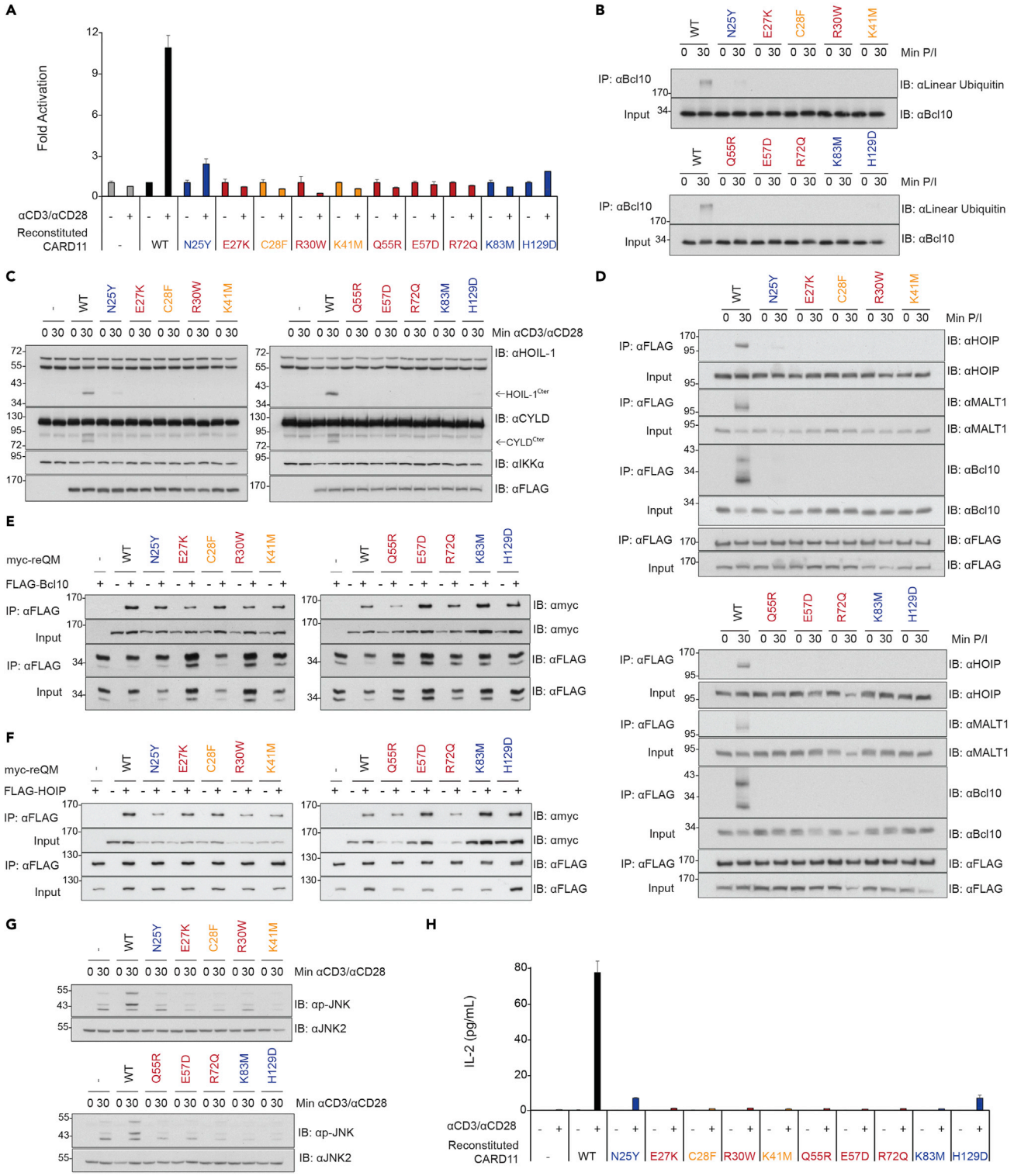

Figure 3. CARD and LATCH domain mutants disrupt the Opening Step in the CARD11 signaling cycle

(A) NF-κB luciferase reporter activity in CARD11-KO Jurkat T cells stably expressing myc-WT-FLAGx2 or myc-mutant-FLAGx2 CARD11 variants via retroviral transduction after stimulation with anti-CD3/anti-CD28 for 4 h. Mean fold activation with SD from one of two replicate experiments is represented. A two-tailed unpaired Student's t test with Welch's correction resulted in the following p values for the values of the CARD11 mutants obtained under stimulated

Figure 3. *Continued*

conditions as compared with that observed for wild-type CARD11 under stimulated conditions: N25Y, p = 0.0252; E27K, p = 0.0405; C28F, p = 0.0399; R30W, p = 0.0388; K41M, p = 0.0399; Q55R, p = 0.0396; E57D, p = 0.0322 R72Q, p = 0.0406; K83M, p = 0.0407; and H129D, p = 0.0245.

(B) CARD11-KO Jurkat T cells reconstituted with myc-WT-FLAGx2 or myc-mutant-FLAGx2 were stimulated with PMA/ionomycin for 30 min, followed by the denatured co-immunoprecipitation assay with rabbit anti-Bcl10 and Western blotting for linear ubiquitin and Bcl10.

(C) Reconstituted cells were stimulated with anti-CD3/anti-CD28 cross-linking for 30 min followed by Western blotting for CYLD, HOIL-1, and the loading controls IKKα and FLAG. The CYLD and HOIL-1 C-terminal cleavage products ($CYLD^{Cter}$ and $HOIL\text{-}1^{Cter}$) are indicated by arrows.

(D) Reconstituted cells were stimulated with PMA/ionomycin for 30 min, followed by the endogenous co-immunoprecipitation assay with rabbit anti-FLAG and Western blotting for HOIP, MALT1, Bcl10, and FLAG.

(E and F) Constructs expressing CARD11 mutants in the constitutively open and active myc-tagged RE Quadruple Mutant (myc-reQM) context were transiently transfected in HEK293T cells with (E) 200 ng FLAG-Bcl10 or (F) 100 ng FLAG-HOIP for co-immunoprecipitation assays. At 40–41 h, cells were lysed and co-immunoprecipitated with rabbit anti-FLAG followed by Western blotting with anti-myc and anti-FLAG. The following concentrations of DNA were used to achieve roughly equivalent protein expression for the FLAG-Bcl10 co-immunoprecipitation: 400 ng reQM, 575 ng N25Y-reQM, 600 ng E27K-reQM, 600 ng C28F-reQM, 675 ng R30W-reQM, 575 ng K41M-reQM, 650 ng Q55R-reQM, 400 ng E57D-reQM, 700 ng R72Q-reQM, 400 ng K83M-reQM, and 450 ng H129D-reQM. The following concentrations of DNA were adjusted to achieve roughly equivalent protein levels for the FLAG-HOIP co-immunoprecipitation: 500 ng reQM in the left panel and 400 ng reQM in the right panel, 500 ng of each reQM mutant.

(G) CARD11-KO Jurkat T cells stably reconstituted with myc-WT-FLAGx2 or myc-mutant-FLAGx2 were stimulated with anti-CD3/anti-CD28 for 30 min followed by Western blotting to detect p-JNK and JNK2.

(H) Reconstituted CARD11-KO Jurkat T cells were stimulated with anti-CD3/anti-CD28 for 24 h and IL-2 production was measured by ELISA. Data are represented as mean pg/mL of IL-2 with SD for one representative experiment performed with three technical replicates. A two-tailed unpaired Student's t test with Welch's correction resulted in the following p values for the values of the CARD11 mutants obtained under stimulated conditions as compared with that observed for wild-type CARD11 under stimulated conditions: N25Y, p = 0.0027; E27K, p = 0.0024; C28F, p = 0.0024; R30W, p = 0.0024; K41M, p = 0.0024; Q55R, p = 0.0024; E57D, p = 0.0024 R72Q, p = 0.0024; K83M, p = 0.0024; and H129D, p = 0.0016.

CYLD by Western blotting. We observed severe defects in inducible MALT1 protease activity in cells expressing each CARD11 mutant and again observed slightly weaker defects in cells expressing N25Y and H129D (Figure 3C).

The deleterious effect of these CARD11 mutations on $LinUb_n$-Bcl10 production and MALT1 protease activation could be due to an inability upstream of the Enzyme Activation Step to specifically support either the TCR-induced conversion of CARD11 from a closed, inactive scaffold to an open, active state during the Opening Step, or the recruitment of signaling cofactors to CARD11 at the subsequent Cofactor Association Step. We therefore assessed the ability of the stably expressed FLAG-tagged CARD11 variants to associate with HOIP, Bcl10, and MALT1 in a signal-inducible manner by stimulating reconstituted cells with PMA and ionomycin for 30 min and performing anti-FLAG co-immunoprecipitation studies. While wild-type CARD11 inducibly recruited HOIP, MALT1 and Bcl10 as expected, all LOF CARD11 variants exhibited severe defects in the recruitment of all three cofactors (Figure 3D). Previous studies have determined that Bcl10 and HOIP associate with CARD11 with different domain requirements, while MALT1 is recruited to CARD11 through Bcl10. Although Bcl10 recruitment depends on both the CARD and Coiled-coil domains (McCully and Pomerantz, 2008), HOIP recruitment depends only on the Coiled-coil domain (Yang et al., 2016). The fact that these mutations in the CARD and LATCH domains affected both Bcl10 and HOIP binding suggested to us that they affected the Opening Step, rather than dramatically disrupting the protein–protein interfaces that bind Bcl10 and HOIP at the Cofactor Association Step.

To confirm this notion, we analyzed the effect of each mutation on the binding of Bcl10 and HOIP to a constitutively open variant of CARD11 in which all four redundant REs are mutated, the RE Quadruple Mutant, or reQM (Wang et al., 2019), a construct originally referred to as re1 re2 re3 re4 (Jattani et al., 2016a). The reQM variant is constitutively active in signaling NF-κB in both lymphoid and nonlymphoid cells and represents CARD11 subsequent to the Opening Step. We reasoned that mutations that affect the Opening Step should have a greater impact in the context of full-length CARD11 on the signal-inducible binding of Bcl10 and HOIP binding than in the context of reQM, which is constitutively open and presents protein surfaces for Bcl10 and HOIP binding without the need for the upstream signaling that neutralizes the REs. We transiently transfected myc-tagged wild-type or mutant reQM constructs into HEK293T cells with FLAG-Bcl10 or FLAG-HOIP and performed anti-FLAG co-immunoprecipitations. All mutants were competent for binding to Bcl10 and HOIP in this assay (Figures 3E and 3F), although quantitation revealed that some mutants did appear to be less efficient at binding Bcl10 than wild-type CARD11 (Table 2). However, for each of the mutants assayed, the relative effect on signal-inducible Bcl10 and HOIP binding in the full-length CARD11 context was greater than that observed in the reQM context (Table 2), arguing that these mutants affect the Opening Step in the CARD11 signaling cycle.

Table 2. Effect of CARD and LATCH LOF mutations on HOIP and Bcl10 binding under inducible and constitutive conditions

CARD11 mutations	Relative Inducible binding full length CARD11:HOIP[a]	Relative constitutive binding reQM CARD11:HOIP[b]	Relative inducible binding full length CARD11:Bcl10[a]	Relative constitutive binding reQM CARD11:Bcl10[b]
WT	1.00	1.00	1.00	1.00
N25Y	0.11	0.81	0.05	0.88
E27K	ND	1.66	ND	0.46
C28F	ND	1.34	ND	0.73
R30W	ND	1.45	ND	0.47
K41M	ND	1.36	ND	0.70
Q55R	ND	3.11	ND	0.37
E57D	ND	1.40	ND	1.50
R72Q	ND	1.53	ND	1.22
K83M	ND	1.13	ND	1.01
H129D	ND	1.09	ND	0.95

[a]Relative inducible binding was calculated by determining the bound/input ratio for each cofactor in CARD11-KO Jurkat T cells expressing full-length LOF CARD11 variants and normalizing to that observed in cells expressing full-length wild-type CARD11 when cells were stimulated with PMA/ionomycin for 30 min after densitometric analysis of the blots in Figure 3D. ND, not detected.

[b]Relative constitutive binding was calculated by determining the bound/input ratio for the reQM CARD11 variants in HEK293T cells and normalizing to that observed in HEK293T cells expressing reQM CARD11 after densitometric analysis of the blots in Figures 3E and 3F.

We also examined the ability of this panel of ten CARD11 variants to support TCR signaling to JNK2 and to the production of IL-2, a known target of TCR signaling that depends on several transcription factors, including NF-κB, NFAT, and AP-1. All mutants displayed defective activation of the JNK2 pathway, as assessed by Western blotting of lysates from anti-CD3/anti-CD28 treated cells with anti-phospho-JNK (Figure 3G). In addition, the anti-CD3/anti-CD28-elicited production of IL-2, as measured by ELISA from cell supernatants, was also severely defective downstream of all CARD11 mutants analyzed, with slightly weaker defects in cells expressing N25Y and H129D (Figure 3H). The data are consistent with each of these ten mutations deleteriously affecting the Opening Step and all subsequent steps in TCR-induced CARD11 signaling when assembling in all-mutant oligomers.

Poisoning of mixed CARD11 oligomers by strong dominant-negative mutants at the Opening Step

We next sought to determine whether strong and weak dominant-negative LOF CARD11 mutants differentially affect the Opening Step or subsequent steps in the CARD11 signaling cycle when co-expressed with wild-type CARD11 and thus populating mixed CARD11 oligomers. To do so, we used retroviral infection to stably express three strong (R30W, R72Q, E27K) and three weak (N25Y, K83M, H129D) dominant negative, FLAG-tagged mutants in wild-type Jurkat T cells where they would form mixed oligomers with the wild-type endogenous CARD11. To assay the Opening Step, we assessed the inducible association of Bcl10 and HOIP with CARD11 following the treatment of cells with PMA/ionomycin, as revealed in anti-Bcl10 and anti-FLAG immunoprecipitates. Interestingly, the inducible binding of Bcl10 to mixed CARD11 oligomers was readily detected with oligomers containing the weak dominant-negative mutants N25Y, K83M, and H129D, but not detected with the strong dominant-negative mutants R30W, R72Q, or E27K (Figure 4A). Thus, although all of these LOF mutants were similarly incapable of inducibly binding Bcl10 in all-mutant oligomers (Figure 3D), the weak dominant negatives did not completely block Bcl10 binding to mixed wild-type:mutant oligomers while the strong dominant negatives did. We observed a similar result for signal-induced HOIP association; inducible HOIP binding to mixed wild-type:mutant oligomers was detectable with oligomers containing weak dominant-negative mutants, but not detectable with strong dominant-negative mutants (Figure 4B). The data indicate that strong and weak dominant-negative LOF CARD11 mutants differentially affect the Opening Step in CARD11 signaling when populating mixed oligomers.

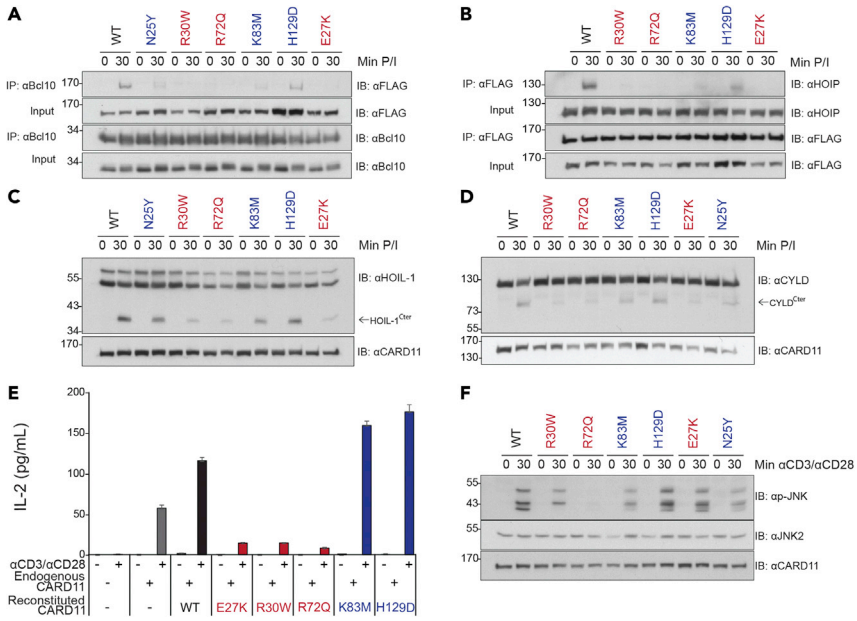

Figure 4. Dominant-negative variants perturb the ability of the mixed wild-type:mutant CARD11 oligomer to proceed through the Opening Step of the CARD11 signaling cycle

(A and B) WT Jurkat T cells that were stably reconstituted with myc-WT-FLAGx2 or myc-mutant-FLAGx2 were stimulated with PMA/ionomycin for 30 min, followed by the endogenous co-immunoprecipitation with (A) anti-Bcl10 and Western blotting for FLAG and Bcl10 or (B) anti-FLAG and Western blotting for HOIP and FLAG. The quantitated relative amounts of FLAG-tagged CARD11 variants in the IP samples from stimulated cells normalized to that in the input lysate for the endogenous Bcl10 IP are the following: WT 1.00, N25Y 0.14, R30W ND, R72Q ND, K83M 0.11, H129D 0.18, and E27K ND, where ND is not detected. The quantitated relative amounts of HOIP proteins in the IP samples from stimulated cells normalized to that in the input lysate for the endogenous FLAG IP are the following: WT 1.00, R30W 0.05, R72Q ND, K83M 0.25, H129D 0.83, and E27K ND, where ND is not detected.

(C and D) MALT1 protease activation at 30 min was assessed by Western blot analysis of input samples from the endogenous anti-Bcl10 co-immunoprecipitation for CARD11 and (C) HOIL-1 or (D) CYLD. The C-terminal cleavage products (HOIL-1^{Cter} and CYLD^{Cter}) are indicated by arrows. The quantitated relative amounts of HOIL-1^{Cter} in stimulated cells normalized to the CARD11 control are the following: WT 1.00, N25Y 0.61, R30W 0.21, R72Q 0.16, K83M 0.45, H129D 0.81, and E27K 0.17. The quantitated relative amounts of CYLD^{Cter} in stimulated cells normalized to the CARD11 control are the following: WT 1.00, R30W 0.30, R72Q 0.42, K83M 0.86, H129D 1.63. E27K 0.65, and N25Y 1.31.

(E) Stably reconstituted WT Jurkat T cells were stimulated with anti-CD3/anti-CD28 for 24 h and IL-2 production was measured by ELISA. Results are the average of replicate experiments and are represented as mean pg/mL IL-2 with SD. A two-tailed unpaired Student's t test with Welch's correction resulted in p values of $p < 0.0001$ for the values of all CARD11 mutants obtained under stimulated conditions as compared with that observed for WT CARD11 under stimulated conditions.

(F) Stably reconstituted WT Jurkat T cells were stimulated with anti-CD3/anti-CD28 for 30 min followed by Western blotting for p-JNK, JNK2, and CARD11. The quantitated relative amounts of p-JNK in stimulated cells normalized to the JNK2 control are the following: WT 1.00, R30W 0.47, R72Q 0.05, K83M 0.40, H129D 1.07, E27K 1.24, and N25Y 0.62.

Consistent with an effect on the Opening Step, mixed CARD11 oligomers containing weak dominant negatives were more active than mixed oligomers containing strong dominant negatives in the ability to support PMA/ionomycin-induced MALT1-proteolytic activity, as assessed by HOIL-1 and CYLD cleavage (Figures 4C and 4D), and anti-CD3/anti-CD28-induced IL-2 production (Figure 4E). Surprisingly, however, there was no such correlation in the activation of JNK signaling downstream of mixed CARD11 oligomers (Figure 4F). Different LOF mutants differentially affected the appearance of phospho-JNK in response to anti-CD3/anti-CD28 treatment regardless of their dominant-negative status in signaling to NF-κB, with R72Q showing the strongest dominant-negative impact on JNK signaling but H129D and E27K showing the least impact (Figure 4F).

Oligomer poisoning by dominant-negative CARD11 mutants can impact a step distinct from the Opening Step

To explore the possibility that all strong dominant-negative LOF CARD11 mutants would target the Opening Step and not other signaling steps, we studied the effect of ten LOF mutations on NF-κB activation in the

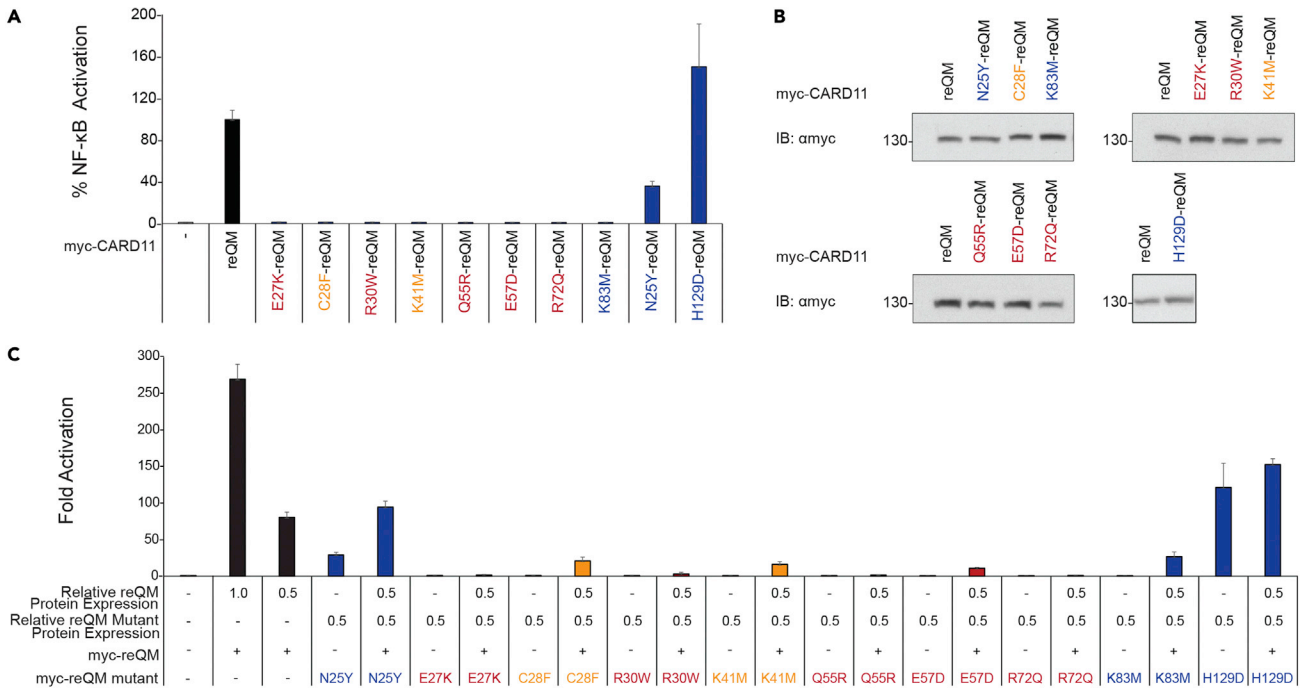

Figure 5. Dominant-negative variants can disrupt a step in the CARD11 signaling cycle subsequent to the Opening Step

(A) NF-κB luciferase reporter activity in CARD11-KO Jurkat T cells transiently transfected with myc-reQM or myc-reQM variants at equivalent protein levels. Relative activity is depicted as a percent of the NF-κB activation achieved with reQM, which corresponds to a fold activation of 80.5, with the mean and SD from one replicate experiment indicated. Mutants are color-coded according to the dominant-negative strength determined in the full-length CARD11 context in Figure 2 and Table 1. A two-tailed unpaired Student's t test with Welch's correction resulted in the following p values for the values of the reQM CARD11 mutants as compared with that observed for reQM CARD11: N25Y-reQM, p = 0.0016; E27K-reQM, p = 0.0027; C28F-reQM, p = 0.0027; R30W-reQM, p = 0.0026; K41M-reQM, p = 0.0026; Q55R-reQM, p = 0.0026; E57D-reQM, p = 0.0026; R72Q-reQM, p = 0.0027; K83M-reQM, p = 0.0026; and H129D-reQM, p = 0.1617.

(B) Anti-myc Western blotting for myc-reQM variants at equivalent protein levels determined by transient transfection of HEK293T cells and the β-galactosidase assay to normalize for transfection efficiency and extract recovery. The following concentrations of DNA were used to achieve roughly equivalent protein level: 90 ng reQM, 450 ng N25Y-reQM, 350 ng E27K-reQM, 300 ng C28F-reQM, 350 ng R30W-reQM, 450 ng K41M-reQM, 300 ng Q55R-reQM, 200 ng E57D-reQM, 350 ng R72Q-reQM, 350 ng K83M-reQM, and 450 ng H129D-reQM.

(C) NF-κB luciferase reporter activity in CARD11-KO Jurkat T cells transiently transfected with myc-reQM mutants in the absence and presence of co-expressed myc-reQM at equivalent protein levels. Mean fold activation with SD is represented from one replicate experiment. A two-tailed unpaired Student's t test with Welch's correction resulted in the following p values for the values of the reQM mutants and reQM CARD11 as compared with that observed with reQM CARD11 at 0.5 protein level: N25Y-reQM + reQM, p = 0.0942; E27K-reQM + reQM, p = 0.0025; C28F-reQM + reQM, p = 0.0005; R30W-reQM + reQM, p = 0.0012; K41M-reQM + reQM, p = 0.0007; Q55R-reQM + reQM, p = 0.0027; E57D-reQM + reQM, p = 0.0027; R72Q-reQM + reQM, p = 0.0027; K83M-reQM + reQM, p = 0.0007; and H129D-reQM + reQM, p = 0.0003.

context of the constitutively open and active reQM CARD11 variant. We first assessed their activities in the absence of co-expressed, otherwise wild-type reQM. If each of these mutations impeded the Opening Step, but no other steps in signaling, then they would be expected to have no impact on the robust NF-κB activation by reQM, since reQM represents CARD11 with all four REs neutralized after the Opening Step. We compared the activity of each reQM mutant to activate the Igκ$_2$-IFN-LUC reporter at comparable expression levels after transient transfection into CARD11-KO Jurkat T cells. Surprisingly, nine of these mutations reduced or eliminated the constitutive 81-fold activation of NF-κB elicited by reQM, including N25Y, E27K, C28F, R30W, K41M, Q55R, E57D, R72Q, and K83M (Figures 5A and 5B), indicating that these mutations can deleteriously affect a step subsequent to the Opening Step when populating all-mutant CARD11 oligomers in the open reQM context. In contrast, the H129D mutation did not adversely affect the activity of the reQM variant, indicating that the H129D mutation prevents the Opening Step, but no other step in signaling, in oligomers entirely composed of mutant subunits (Figures 5A and 5B). The data indicate that while N25Y, E27K, C28F, R30W, K41M, Q55R, E57D, R72Q, and K83M can disrupt the Opening Step in the full-length CARD11 context (Figure 3), these mutations can also independently disrupt a step subsequent to the Opening Step when populating all-mutant CARD11 oligomers in the reQM context, assigning to the wild-type residues at these positions at least two distinguishable roles in CARD11 signaling.

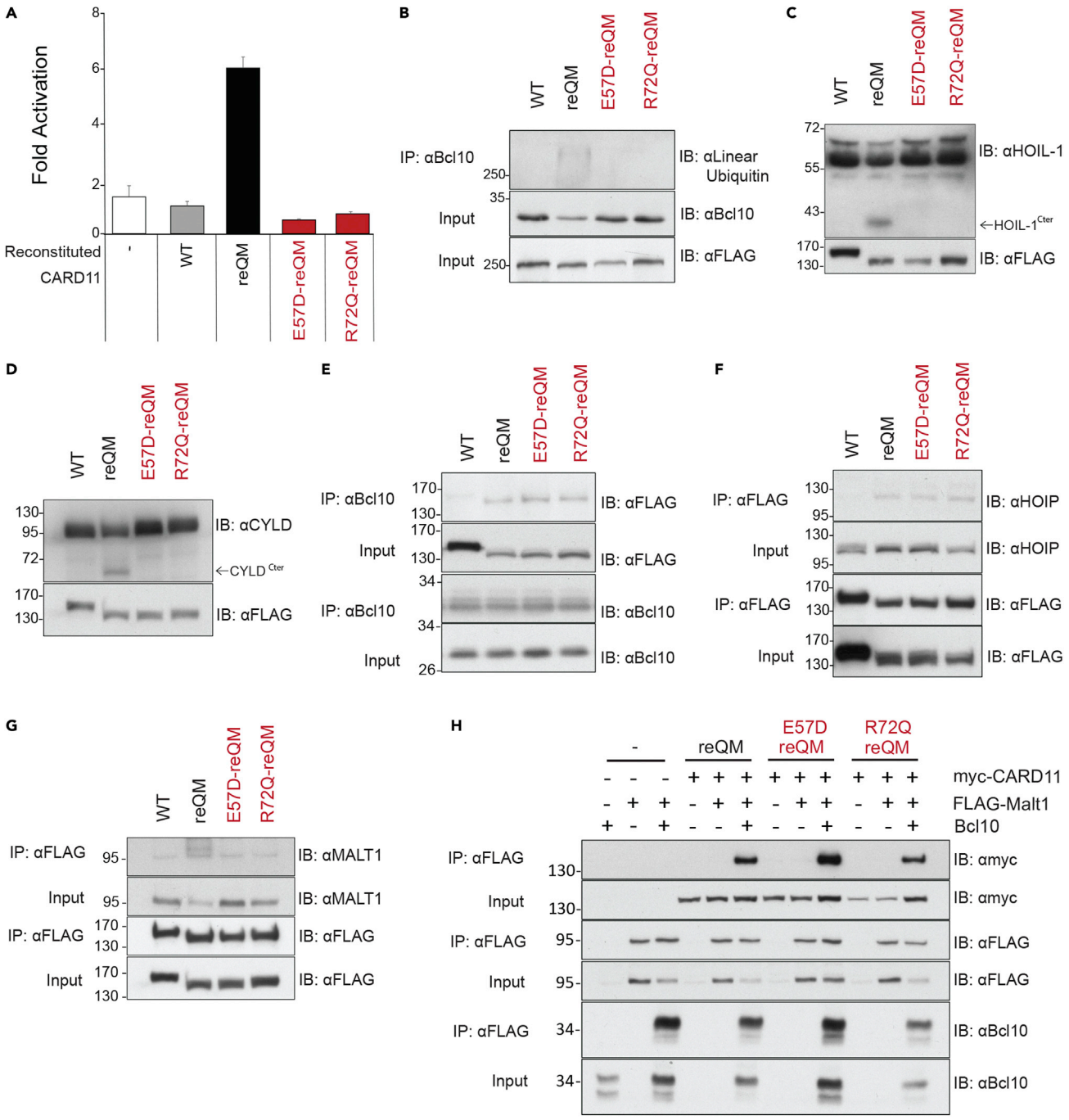

Figure 6. Dominant-negative CARD11 variants in the open, reQM conformation perturb the ability of the all-mutant reQM CARD11 oligomer to recruit MALT1

(A) NF-κB luciferase reporter activity in CARD11-KO Jurkat T cells stably transduced with myc-WT CARD11-FLAGx2 or myc-reQM CARD11-FLAGx2 with or without CARD11 LOF mutations. Mean fold activation with SD is depicted relative to Jurkat T cells reconstituted with WT CARD11. A two-tailed unpaired Student's t test with Welch's correction resulted in the following p values for the reQM CARD11 mutants as compared with that observed for reQM CARD11: E57D-reQM, p = 0.0016; and R72Q-reQM, p = 0.0013.

(B) Reconstituted cells were harvested for denatured co-immunoprecipitation with rabbit anti-Bcl10 and Western blotting for linear ubiquitin, Bcl10, and FLAG.

(C and D) MALT1 protease activation was assessed by Western blot analysis for HOIL-1, CYLD, and FLAG. The HOIL-1 and CYLD C-terminal cleavage products (HOIL-1^{Cter} and CYLD^{Cter}) are indicated by arrows.

Figure 6. *Continued*

(E–G) Cells were harvested for the endogenous co-immunoprecipitation with mouse anti-Bcl10 (E) or rabbit anti-FLAG (F and G) and lysate inputs and immunoprepcipiates were probed by Western blotting with the indicated antibodies.

(H) The myc-reQM CARD11 variants were transiently transfected in HEK293T cells with 500 ng FLAG-MALT1 and 300 ng untagged Bcl10 as indicated for co-immunoprecipitation assays. At 40–41 h, cells were lysed and co-immunoprecipitated with rabbit anti-FLAG followed by Western blotting for myc, FLAG, and Bcl10. The following concentrations of DNA were used to achieve roughly equivalent protein expression for the FLAG-MALT1 co-immunoprecipitation: 400 ng reQM, 375 ng E57D-reQM, and 700 ng R72Q-reQM.

Next, to determine whether any of these mutations could confer dominant-negative activity in mixed reQM oligomers, we co-expressed each reQM variant in the presence of an equivalent amount of otherwise wild-type reQM in CARD11-KO Jurkat T cells. Interestingly, E27K, R30W, Q55R, and R72Q mutants had the strongest dominant-negative activity in the reQM context; they were able to reduce signaling from the co-expressed unmutated reQM variant from 81-fold NF-κB activation when expressed alone to less than 3-fold (Figure 5C). The C28F, K41M, E57D, and K83M variants were of intermediate potency in dominant-negative activity in the reQM context, while N25Y and H129D mutants exhibited the weakest dominant activity, if any, in this assay (Figure 5C). It is clear from these data that a step subsequent to the Opening Step is also susceptible to inhibition by some dominant-negative CARD11 mutants when present in mixed wild-type:mutant oligomers.

Disruption of signal-induced MALT1 association with CARD11 by E57D and R72Q mutations

Our next goal was to identify one or more of the steps after Opening that are susceptible to dominant-negative inhibition. We chose to further investigate the E57D and R72Q mutants since they appeared to have the least effect on Bcl10 and HOIP binding to the constitutively open reQM variant among the panel we analyzed previously after expression in HEK293T cells (Figures 3E and 3F, Table 2), and therefore might uncover a previously unrecognized role for the CARD11 CARD domain in signaling. We used retroviral infection to stably reconstitute CARD11-KO Jurkat T cells with either FLAG-tagged wild-type CARD11, the reQM variant, E57D-reQM, or R72Q-reQM. As expected, the reQM variant elicited constitutive activation of the Igκ$_2$-IFN-LUC reporter in unstimulated cells while wild-type CARD11 did not (Figure 6A) and the reQM activity was abrogated by the E57D and R72Q mutations (Figure 6A). As shown previously (Wang et al., 2019), reQM expression resulted in the spontaneous production of LinUb$_n$-Bcl10 (Figure 6B) and cleavage of HOIL-1 (Figure 6C) and CYLD (Figure 6D), reflecting the induction of HOIP and MALT1 enzymatic activity in the Enzyme Activation Step. Interestingly, both E57D and R72Q mutations prevented these activities (Figures 6B, 6C, and 6D). We next probed for the constitutive association of Bcl10 and HOIP in co-immunoprecipitation assays and found that the parental reQM, E57D-reQM, and R72Q-reQM all associated with Bcl10 and HOIP with equivalent efficiencies (Figures 6E and 6F), suggesting that the E57D and R72Q mutations disrupted a step between Bcl10 and HOIP binding and the activation of HOIP and MALT1 enzymatic activities. We next probed for MALT1 association. Interestingly, reQM showed a greater constitutive association with MALT1 than either E57D-reQM or R72Q-reQM (Figure 6G), especially for several slower migrating species of MALT1 that have been extensively and elegantly characterized by others as resulting from the signal-inducible phosphorylation and ubiquitinylation of MALT1 (Duwel et al., 2009; Gehring et al., 2019; Oeckinghaus et al., 2007; Pelzer et al., 2013; Schairer et al., 2020). Previous studies have shown that MALT1 is recruited to CARD11 during signaling through Bcl10 (Juilland and Thome, 2018; Meininger and Krappmann, 2016). The observed defect in MALT1 association with E57D-reQM and R72Q-reQM mutants might be due to effects of these mutations to alter the conformation of Bcl10 bound to CARD11 in such a manner that MALT1 cannot associate as well, or alternatively, the E57D and R72Q mutations may disable a capability of the reQM that either recognizes or actively promotes the phosphorylation and ubiquitinylation of MALT1 that are known to occur in T cells and make MALT1 more stably associate with the CBM complex (Duwel et al., 2009; Gehring et al., 2019; Oeckinghaus et al., 2007; Pelzer et al., 2013; Schairer et al., 2020). We therefore overexpressed FLAG-MALT1, untagged Bcl10, and myc-tagged reQM, E57D-reQM, and R72Q-reQM in HEK293T cells and assayed the relative ability of MALT1 to co-IP with reQM variants in a Bcl10-dependent manner. In this assay (Figure 6H), E57D-reQM and R72Q-reQM showed no defect in the ability to recruit MALT1 in a Bcl10-dependent manner, suggesting that E57D and R72Q do not directly perturb the protein–protein interfaces required for CARD11:Bcl10:MALT ternary complex formation after overexpression in nonlymphoid cells. Rather, the data suggest that the E57D-reQM and R72Q-reQM mutants may be defective for signaling in the T cell environment that leads to MALT1 modification and sustained MALT1 association with CARD11 and Bcl10 or defective in the specific recognition and recruitment of modified MALT1 in the CBM complex in T cells.

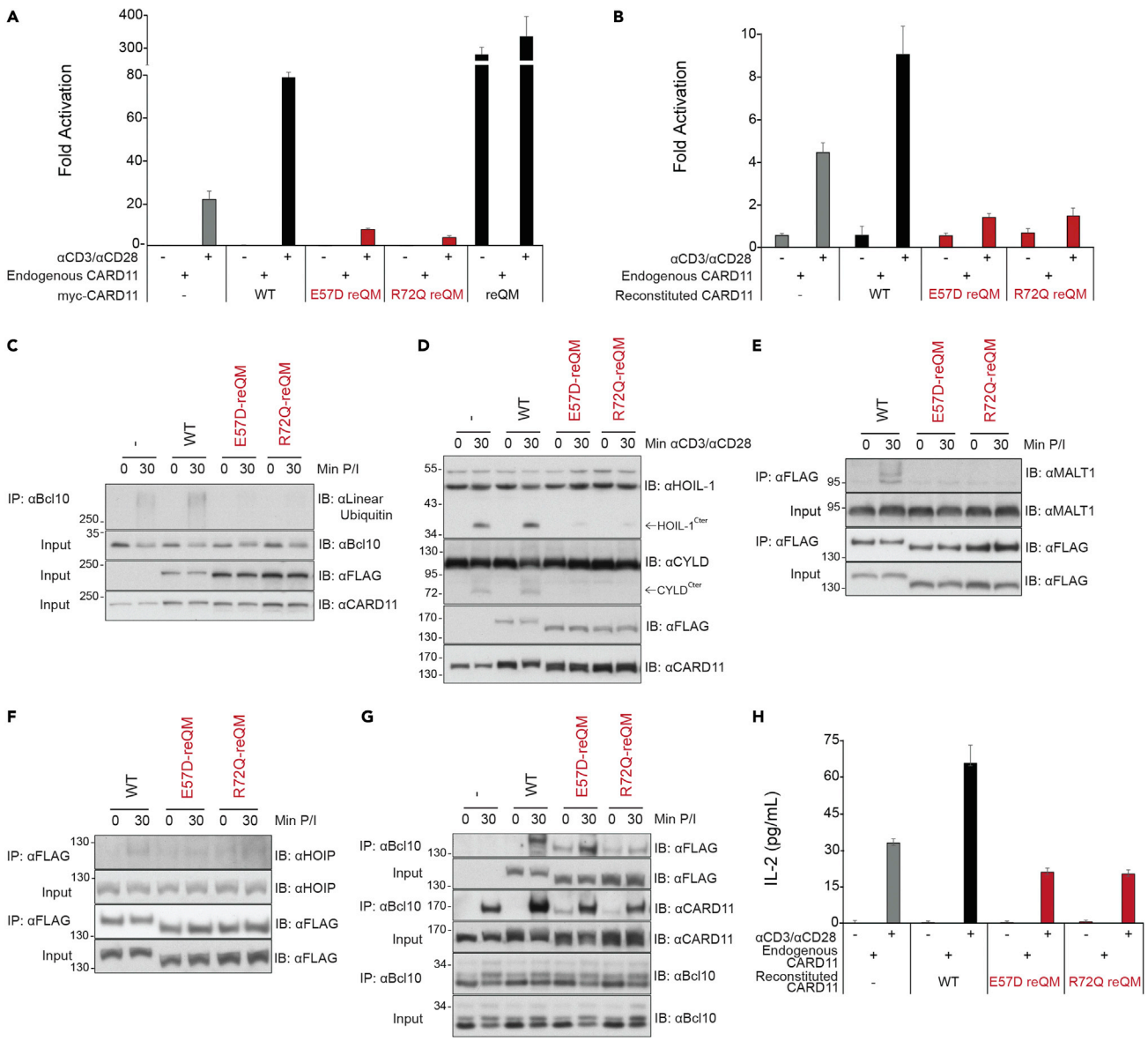

Figure 7. Dominant-negative variants in the open, reQM conformation perturb the ability of the mixed wild-type:reQM mutant CARD11 oligomers to inducibly recruit cofactors

(A) NF-κB luciferase reporter activity in WT Jurkat T cells transiently transfected with 100 ng of myc-WT CARD11 or 100ng myc-reQM CARD11 with or without dominant-negative mutations. Mean fold activation with SD is depicted relative to unstimulated wild-type Jurkat T cells. A two-tailed unpaired Student's t test with Welch's correction resulted in the following p values for stimulated cells expressing reQM variants as compared with that observed for WT CARD11: E57D-reQM, p = 0.0002; R72Q-reQM, p < 0.0001; and reQM, p = 0.0145.

(B) NF-κB luciferase reporter activity in WT Jurkat T cells stably reconstituted with myc-WT CARD11-FLAGx2, myc-E57D-reQM-FLAGx2, or myc-R72Q-reQM CARD11-FLAGx2. Mean fold activation with SD is depicted relative to unstimulated Jurkat T cells reconstituted with an empty vector. A two-tailed unpaired Student's t test with Welch's correction resulted in the following p values for the values of cells reconstituted with CARD11 variants as compared with that observed for WT Jurkat cells without CARD11 reconstitution under stimulated conditions: WT, p = 0.0043, E57D-reQM, p = 0.0008; and R72Q-reQM, p = 0.0001.

(C) Wild-type Jurkat T cells that were stably reconstituted with myc-WT-FLAGx2 or myc-reQM-FLAGx2 variants were harvested for the denatured co-immunoprecipitation with rabbit anti-Bcl10 and Western blotting for linear ubiquitin, Bcl10 FLAG, and CARD11.

(D) MALT1 protease activation was assessed by Western blot analysis for HOIL-1, CYLD, FLAG, and CARD11. The HOIL-1 and CYLD C-terminal cleavage products (HOIL-1^{Cter} and CYLD^{Cter}) are indicated by the arrows.

(E–G) Cells were harvested for the endogenous co-immunoprecipitation with rabbit anti-FLAG (E and F) or mouse anti-Bcl10 (G) and lysate inputs and immunoprecipitates were probed by Western blotting for the indicated antibodies.

Figure 7. *Continued*

(H) WT Jurkat T cells stably reconstituted with WT or reQM mutants were stimulated with anti-CD3/anti-CD28 for 24 h and IL-2 production was measured by ELISA. Results are the representative of one replicate experiment and are represented as mean pg/mL IL-2 with SD. A two-tailed unpaired Student's t test with Welch's correction resulted in the following p values for cells reconstituted with CARD11 variants as compared with that observed for WT Jurkat cells without CARD11 reconstitution under stimulated conditions: WT, p = 0.0134, E57D-reQM, p = 0.0009; and R72Q-reQM, p = 0.0007.

We next assessed whether the E57D-reQM and R72Q-reQM mutants could block signaling from the endogenous wild-type CARD11 in Jurkat T cells and whether these mutants would reduce the recruitment of modified MALT1 to mixed wild-type:mutant CARD11 oligomers. In a transient transfection assay, both E57D-reQM and R72Q-reQM significantly reduced the activation of the Igκ_2-IFN-LUC reporter after anti-CD3/anti-CD28 stimulation (Figure 7A), consistent with an ability to interfere with signaling from the endogenous wild-type CARD11. We then stably expressed FLAG-tagged wild-type CARD11, E57D-reQM, and R72Q-reQM in parental Jurkat T cells via retroviral transduction. As expected, the expression of E57D-reQM and R72Q-reQM in these cells dominantly interfered with the induction of the Igκ_2-IFN-LUC reporter following treatment with anti-CD3/anti-CD28 (Figure 7B). Expression of these reQM variants also reduced the signal-inducible generation of LinUb$_n$-Bcl10 (Figure 7C) and HOIL-1 and CYLD cleavage (Figure 7D), consistent with a dominant-negative effect of these constitutively open variants upstream of the activation of HOIP and MALT1 enzymatic activity. We next probed for MALT1 recruitment to the mixed oligomers in these cells during signaling. We detected the inducible recruitment of modified MALT1 species to wild-type CARD11 oligomers only after treatment with PMA/ionomycin (Figure 7E), while no modified MALT1 association was observed for E57D-reQM and R72Q-reQM containing oligomers in either unstimulated or stimulated cells (Figure 7E). Both E57D-reQM and R72Q-reQM containing mixed oligomers constitutively associated with HOIP in unstimulated cells (Figure 7F). After PMA/ionomycin treatment, HOIP association increased with R72Q-reQM containing oligomers, presumably due to the opening of wild-type full-length subunits in the oligomers, but this increase was less pronounced with E57D-reQM containing oligomers (Figure 7F). Bcl10 constitutively associated with both E57D-reQM and R72Q-reQM containing oligomers in unstimulated cells (Figure 7G), while PMA/ionomycin-inducible Bcl10 association was partially reduced in cells expressing both E57D-reQM and R72Q-reQM mutants, with a larger effect observed for mixed oligomers containing the R72Q-reQM mutant. The results are consistent with the ability of E57D and R72Q mutants in mixed oligomers to interfere during signaling with the Cofactor Association Step following TCR triggering, with a dramatic effect on modified MALT1 binding to CARD11 and a partial effect on Bcl10 or HOIP. The partial effects of E57D-reQM and R72Q-reQM mutants on Bcl10 and HOIP binding that we observed in these cells after PMA/ionomycin treatment were different from the lack of effects on Bcl10 and HOIP binding to all mutant E57D-reQM and R72Q-reQM oligomers that we observed in Figure 6 without PMA/ionomycin treatment. This difference suggests that PMA/ionomycin, which mimics upstream signaling from the TCR and from costimulatory receptors, induces events that maximize Bcl10 and HOIP binding to CARD11 in a manner that is not fully supported by the E57D and R72Q mutants. Finally, consistent with their dominant-negative capabilities in the constitutively open reQM context, both E57D-reQM and R72Q-reQM expression significantly interfered with IL-2 production in these cells downstream of anti-CD3/anti-CD28 treatment (Figure 7H).

DISCUSSION

The CARD11 signaling scaffold is remarkably susceptible to different classes of germline mutations that can impair lymphocyte activation and precipitate immunodeficiency. These include the homozygous LOF mutations observed in CARD11 deficiency, the heterozygous GOF mutations in BENTA, and the heterozygous dominant-negative LOF mutations in CADINS. The impact of these mutations is due to the central signaling role that CARD11 plays in antigen receptor signaling to NF-κB, mTOR, and JNK. However, it has remained mechanistically unclear what distinguishes strong dominant-negative LOF mutants that manifest disease when heterozygous from those LOF mutants that do so only when homozygous.

Strong dominant-negative mutants are those most capable of poisoning signaling from the mixed wild-type:mutant CARD11 oligomers that assemble in lymphocytes that are heterozygous for the LOF allele. Our results indicate that at least two steps in the CARD11 signaling cycle can be deleteriously affected by dominant-negative variants in this manner, the Opening Step, in which CARD11 is inducibly converted from a closed, inactive state to an open and active scaffold downstream of antigen receptor triggering, and the Cofactor Association Step, in which cofactors bind to CARD11 once its interaction surfaces become accessible after opening (Figure 8).

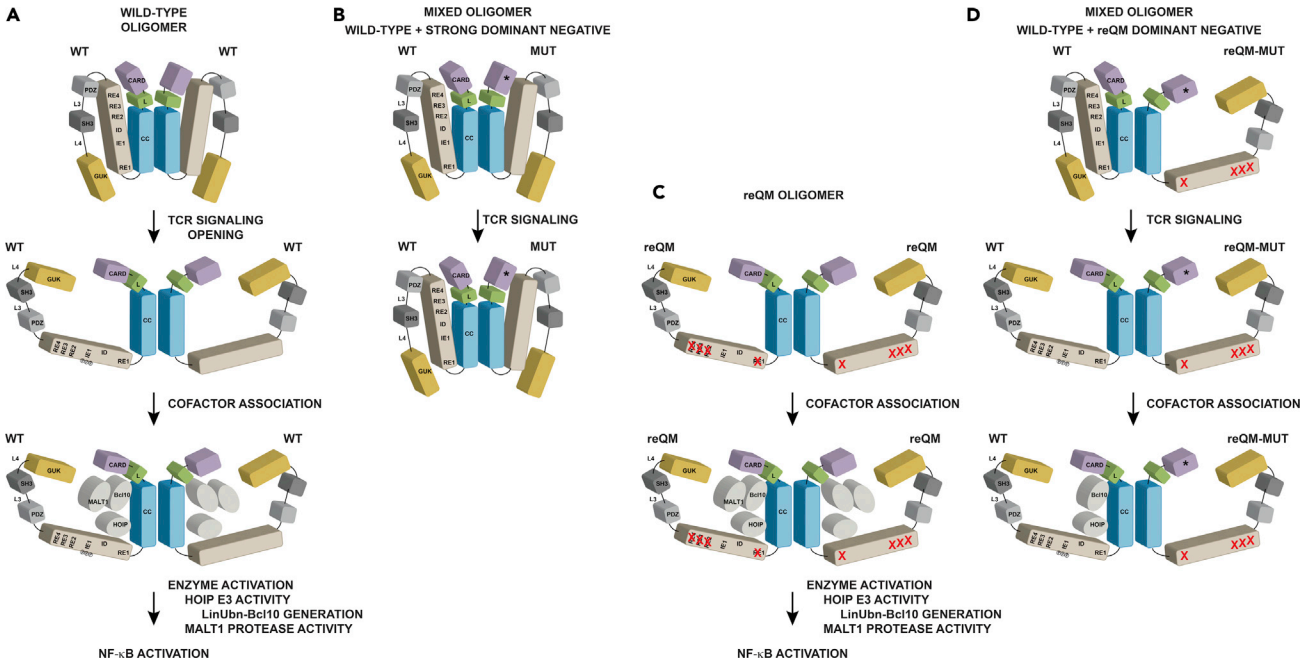

Figure 8. Model illustrating two steps impacted by dominant-negative CARD11 mutations in TCR signaling

(A) CARD11 exists as an oligomer of unknown stoichiometry of at least 2 subunits in a closed conformation in the absence of antigen receptor signaling. Upon TCR signaling all wild-type (WT) CARD11 oligomers become active and proceed through the Opening, Cofactor Association, and Enzyme Activation Steps leading to the transient activation of NF-κB.

(B) Mixed wild-type:mutant oligomers containing a strong dominant-negative mutant cannot proceed through the Opening Step, causing the oligomer to stay in the closed conformation following TCR signaling.

(C) Oligomers consisting of the constitutively open reQM variant with all four REs disabled constitutively proceed through the Cofactor Association and Enzyme Activation Steps leading to constitutive activation of NF-κB.

(D) Mixed wild-type:mutant reQM oligomers containing E57D or R72Q mutations fail to recruit MALT1 and optimally recruit HOIP and Bcl10 at the Cofactor Association Step.

The effect of mutants at the Opening Step is likely sufficient to account for dominant-negative activity for the mutants we studied since the Opening Step is required during signaling as a prerequisite for all subsequent steps. This effect on opening explains why strong dominant-negative mutations can prevent the inducible association of CARD11 with several cofactors that associate with CARD11 through independent determinants in the N-terminal half of CARD11. However, it is striking that the strong dominant-negative mutations we studied affect both opening and a subsequent step, indicating that the respective wild-type residues must participate in two or more steps during the CARD11 signaling cycle. This dual role of residues is reminiscent of the role for residues in IE1 that participate in both the Opening and Enzyme Activation Steps (Wang et al., 2019) and reinforces the notion that individual CARD11 residues coordinate at least two steps in signaling likely to ensure that signaling is tightly regulated and concerted. For E57 and R72, our data indicate that in addition to controlling the Opening Step, these residues are also critical at the Cofactor Association Step after opening occurs for both the stable association of MALT1 with CARD11 and to achieve maximal TCR-induced Bcl10 and HOIP binding.

The Opening Step remains a poorly understood key step in lymphocyte activation. It is clear that signals emanating from the antigen receptor somehow result in the neutralization of the four REs in the CARD11 inhibitory domain, which cooperatively keep CARD11 in the inactive state in the absence of receptor triggering, in part via intramolecular interactions that prevent CARD11 binding to cofactors (Jattani et al., 2016a, 2016b). RE neutralization depends on IE1, which resides within the Inhibitory Domain (Wang et al., 2019) and houses three serine residues that are targeted for inducible phosphorylation by PKCθ, PKCβ, IKKβ, and at least one unknown kinase (Matsumoto et al., 2005; Shinohara et al., 2007; Sommer et al., 2005). However, it is still not clear how IE1 is recognized to promote the Opening Step and whether the phosphorylation of IE1 residues is as clearly required as originally modeled (Pomerantz, 2021; Wang et al., 2019). The results in this study reveal intriguing new insights into CARD11 opening and regulation.

First, our analysis of a panel of CARD11 LOF mutants indicates that the CARD and LATCH domains are recognized and participate in the Opening Step. The mutation of residues N25, E27, C28, R30, K41, Q55, E57, R72, and K83 in the CARD, and H129 in the LATCH, prevents the inducible association of Bcl10 and HOIP to CARD11 downstream of TCR triggering, while the same mutations have much less of an effect, if any, on Bcl10 or HOIP binding to the constitutively open reQM variant, indicating a greater role of these residues in making the CARD and Coiled-coil domains accessible for cofactor binding in the Opening Step than in supporting interactions at the CARD11:cofactor protein:protein interface in the Cofactor Association Step. Several structural elements and surfaces of the CARD are important in the Opening Step (Figures 2A and S2), which emphasizes the critical role of this domain in this first step in CARD11 signaling. Second, our analysis of mixed wild-type:mutant oligomers reveals that the deleterious effects of some LOF mutants (N25Y, K83M, H129D) on CARD11 opening can be partially rescued by the presence of wild-type subunits in the oligomer, while the severe effects of other mutants (R30W, R72Q, E27K) cannot. This differential behavior when co-expressed with wild-type CARD11 can explain why some mutants are strong dominant-negative CARD11 variants for NF-κB activation, while others are not. In addition, the analysis suggests that the distinct subunits in the CARD11 oligomer cooperate or coordinate during the Opening Step. In this view, mutations that more severely impede subunit cooperation will poison the oligomer and can manifest disease in the heterozygous state.

Our analysis of constitutively open reQM variants clearly indicates that the Opening Step is not the only step in the CARD11 signaling cycle that can be deleteriously affected by strong dominant-negative mutants in mixed wild-type:mutant CARD11 oligomers. The reQM E27K, R30W, Q55R, and R72Q mutants each severely reduced the constitutive signaling by the co-expressed reQM variant. The reQM C28F, K41M, E57D, and K83M mutants had moderate dominant-negative activity in this assay, while reQM N25Y and H129D had the weakest effects, if any. Our study of the E57D and R72Q mutations in the reQM context indicated a clear impact of these mutations at the Cofactor Association Step, with the most dramatic effect on inducible MALT1 association with CARD11, but also some effect on Bcl10 and HOIP binding in mixed oligomers (Figures 8C and 8D). Extensive studies have shown that MALT1 is ubiquitinylated and phosphorylated during signaling, in part by the E3 ligase TRAF6 and the kinase CK1α, and that these modifications are required for optimal antigen receptor signaling (Duwel et al., 2009; Gehring et al., 2019; Oeckinghaus et al., 2007). Interestingly, these modifications occur after the initial recruitment of Bcl10 and MALT1 to CARD11 in T cells (Gehring et al., 2019). The binding of MALT1 and Bcl10 to CARD11 that we observe in nonlymphoid cells (Figure 6H) likely reflects this initial recruitment of unmodified MALT1. CARD11 residues E57 and R72 in the CARD domain may be involved in promoting kinase and E3 ligase action on MALT1, or they may be involved directly or indirectly in stabilizing the association of modified MALT1 in the CBM complex in T cells. It is possible that effects of E57D and R72Q in the reQM context on MALT1 proteolytic activity and HOIP E3 ligase activity are due to their effects on stable MALT1 recruitment to CARD11. The stable recruitment of MALT1 in the CBM complex may be required for MALT1 cleavage of HOIL-1 and CYLD. MALT1 is required for LinUbn-Bcl10 generation (Yang et al., 2016), and its absence from the CBM complex may prevent its undefined role in that process. The effects of E57D and R72Q mutations on optimal HOIP and Bcl10 binding to CARD11 that appear after PMA/ionomycin treatment, but not appreciably in the reQM context in unstimulated cells, suggests that signaling events upstream of CARD11 may promote Bcl10 and HOIP binding to CARD11 in a manner that is not fully supported by the R72Q and E57D mutations. Meitlis et al. have made similar conclusions for the involvement of R72 in Bcl10 binding consistent with their analysis of several mutations at this position (Meitlis et al., 2020).

It is important to point out that other steps in signaling could be disrupted by dominant-negative CARD11 mutants in mixed wild-type:mutant oligomers, including at other interfaces at the Cofactor Association Step, at the Enzyme Activation Step, or at a previously unrecognized step in CARD11 signaling that also depends on the coordinated action of different subunits in the CARD11 oligomer. Further work will be necessary to fully explain which other steps are perturbed by E27K, C28F, K41M, Q55R, and K83M. We did observe some deleterious effects of E27K, C28F, K41M, and Q55R mutations in Bcl10 binding to the reQM variant (Figure 3E, Table 2), which could be consistent with an effect of these mutations at the Cofactor Association Step. We note that both K41 and R72 have been modeled in silico to reside at the CARD11:Bcl10 interface (Li et al., 2012; Meitlis et al., 2020; Qiao et al., 2013), although no direct structure of this interface has as yet been determined. Although we did not directly examine the effects of dominant-negative CARD11 mutations on signal-induced Bcl10 polymerization into filaments, it is extremely likely that mutations that prevent CARD11 opening or that independently impair Bcl10 binding

to CARD11 will negatively affect filament formation since Bcl10 filaments are thought to be seeded by the recruitment of Bc10 to the CARD11 CARD domain (David et al., 2018; Qiao et al., 2013; Seeholzer et al., 2018).

Our studies focused mainly on CARD11 signaling to NF-κB downstream of TCR triggering, but it is important to consider other CARD11-dependent pathways in the effort to explain why some LOF CARD11 mutations impact patients as dominant negatives while other LOF CARD11 mutations do not. Interestingly, our analysis of CARD11 signaling to JNK indicates that all of the mutants we surveyed that were defective in NF-κB signaling were also defective in signaling to JNK when assembled into all-mutant CARD11 oligomers (Figure 3G). However, when assembled into mixed wild-type:mutant CARD11 oligomers, there was no correlation between a mutant's relative dominant-negative effect on NF-κB signaling and its dominant-negative effect on JNK signaling (Figure 4F). This observation suggests that CARD11 subunits in the CARD11 oligomer operate with different coordination between subunits required for JNK signaling than for NF-κB signaling. Further work will be required to understand exactly how CARD11 signals to JNK and build on previous studies that have examined this branch of CARD11 signaling (Blonska et al., 2007; Blonska and Lin, 2009; Hara et al., 2003; Jun et al., 2003). We also attempted to evaluate the effect of the mutations we studied on CARD11 signaling to mTOR; however, we found that in our hands, mTORC1 activation downstream of TCR cross-linking was not dependent on CARD11 in Jurkat T cells (data not shown), in contrast to previous studies (Hamilton et al., 2014; Nakaya et al., 2014). Mice heterozygous for the R30W mutation observed in CADINS do, however, display modest defects in TCR signaling to mTORC1 in $CD4^+$ T cells (Hutcherson et al., 2021). Since CARD11 dominant-negative mutants exert their effects by interfering with signaling from the co-expressed wild-type CARD11, it is unlikely that these mutants will perturb pathways that are CARD11-independent. For example, inducible ERK phosphorylation, which is known to be CARD11-independent, has been shown to be unaffected by dominant-negative CARD11 mutants in primary T cells (Ma et al., 2017).

It remains to be determined what threshold of CARD11 dominant-negative activity is required to elicit CADINS disease in patients. The increasing identification and study of LOF CARD11 mutations in patients (Dadi et al., 2018; Dorjbal et al., 2019; Greil et al., 2013; Izadi et al., 2021; Lu et al., 2019, 2021; Ma et al., 2017; Stepensky et al., 2013), in model systems (Meitlis et al., 2020), and mice (Hutcherson et al., 2021) promise to accelerate our understanding of the different clinical syndromes associated with different classes of CARD11 mutations.

Limitations of the study

Here, we investigated the mechanisms by which a small number of dominant-negative CARD11 mutations impact signaling downstream of TCR triggering. It is possible that other known and emerging dominant-negative mutations will impact interactions and signaling steps that we did not describe. A full understanding of the mechanistic effects of dominant-negative CARD11 mutations will require the determination of the three dimensional structure of CARD11 in both inactive and active states, which will reveal the stoichiometric context in which dominant-negative mutations perturb signaling from mixed wild-type:mutant oligomers. Furthermore, dominant-negative CARD11 mutations may cause CADINS with differential effects on signaling in different cell types, including T cells, B cells, NK cells, and their different subtypes (see for example Hutcherson et al., 2021)). Further studies will be required to evaluate whether the mechanisms of dominant-negative activity we have uncovered also apply in these different cellular environments in primary cells *in vivo*.

STAR★METHODS

Detailed methods are provided in the online version of this paper and include the following:

- KEY RESOURCES TABLE
- RESOURCE AVAILABILITY
  - Lead contact
  - Materials availability
  - Data and code availability
- EXPERIMENTAL MODEL AND SUBJECT DETAILS
  - Cell lines
- METHODS DETAILS

- Site-directed mutagenesis
- Determination of equivalent CARD11 protein expression in HEK293T cells
- Co-immunoprecipitations in HEK293T cells
- Transient transfection and NF-κB luciferase reporter assay in Jurkat T cells
- Generation and validation of GFP-expressing CARD11-KO Jurkat T cells
- Stable reconstitution of wild-type and CARD11-KO Jurkat T cells with CARD11 variants
- Endogenous co-immunoprecipitation in Jurkat T cells
- Denatured endogenous co-immunoprecipitation in Jurkat T cells
- Determination of MALT1 protease and JNK activation
- IL-2 ELISA

- QUANTIFICATION AND STATISTICAL ANALYSIS
  - Quantification of western blots
  - Statistical analysis

SUPPLEMENTAL INFORMATION

Supplemental information can be found online at https://doi.org/10.1016/j.isci.2022.103810.

ACKNOWLEDGMENTS

We thank N. Carter for critical reading of the manuscript and M. Meffert, Z. Wang, and C. Yang for helpful discussions and advice. This work was supported by the National Institutes of Health grant RO1AI148143 and funds from The Johns Hopkins University School of Medicine Department of Biological Chemistry. J.R.B. was supported by the National Institutes of Health grant T32AI007247. S.M.H. was supported by National Institutes of Health grants T32CA009110 and T32GM007445.

AUTHOR CONTRIBUTIONS

J.L.P. acquired funding, conceived the project, and supervised the research. J.R.B. designed and conducted most of the experiments. N.S. and S.M.H. conducted experiments. J.R.B. and J.L.P. wrote the manuscript. All authors discussed the results and commented on the manuscript.

DECLARATION OF INTEREST

The authors declare no competing interests.

Received: June 11, 2021
Revised: December 10, 2021
Accepted: January 19, 2022
Published: February 18, 2022

REFERENCES

Arjunaraja, S., Angelus, P., Su, H.C., and Snow, A.L. (2018). Impaired control of epstein-barr virus infection in B-cell expansion with NF-kappaB and T-cell anergy disease. Front. Immunol. *9*, 198. https://doi.org/10.3389/fimmu.2018.00198.

Arjunaraja, S., Nose, B.D., Sukumar, G., Lott, N.M., Dalgard, C.L., and Snow, A.L. (2017). Intrinsic plasma cell differentiation defects in B cell expansion with NF-kappaB and T cell anergy patient B cells. Front. Immunol. *8*, 913. https://doi.org/10.3389/fimmu.2017.00913.

Balannik, V., Lamb, R.A., and Pinto, L.H. (2008). The oligomeric state of the active BM2 ion channel protein of influenza B virus. J. Biol. Chem. *283*, 4895–4904. https://doi.org/10.1074/jbc.M709433200.

Bedsaul, J.R., Carter, N.M., Deibel, K.E., Hutcherson, S.M., Jones, T.A., Wang, Z., Yang, C., Yang, Y.K., and Pomerantz, J.L. (2018). Mechanisms of regulated and dysregulated CARD11 signaling in adaptive immunity and disease. Front. Immunol. *9*, 2105. https://doi.org/10.3389/fimmu.2018.02105.

Blonska, M., and Lin, X. (2009). CARMA1-mediated NF-kappaB and JNK activation in lymphocytes. Immunol. Rev. *228*, 199–211. https://doi.org/10.1111/j.1600-065X.2008.00749.x.

Blonska, M., Pappu, B.P., Matsumoto, R., Li, H., Su, B., Wang, D., and Lin, X. (2007). The CARMA1-Bcl10 signaling complex selectively regulates JNK2 kinase in the T cell receptor-signaling pathway. Immunity *26*, 55–66. https://doi.org/10.1016/j.immuni.2006.11.008.

Brohl, A.S., Stinson, J.R., Su, H.C., Badgett, T., Jennings, C.D., Sukumar, G., Sindiri, S., Wang, W., Kardava, L., Moir, S., et al. (2014). Germline CARD11 mutation in a patient with severe congenital B cell lymphocytosis. J. Clin. Immunol. *35*, 32–46. https://doi.org/10.1007/s10875-014-0106-4.

Buchbinder, D., Stinson, J.R., Nugent, D.J., Heurtier, L., Suarez, F., Sukumar, G., Dalgard, C.L., Masson, C., Parisot, M., Zhang, Y., et al. (2015). Mild B-cell lymphocytosis in patients with a CARD11 C49Y mutation. J. Allergy Clin. Immunol. *136*, 819–821. https://doi.org/10.1016/j.jaci.2015.03.008.

Chan, W., Schaffer, T.B., and Pomerantz, J.L. (2013). A quantitative signaling screen identifies CARD11 mutations in the CARD and LATCH domains that induce Bcl10 ubiquitination and human lymphoma cell survival. Mol. Cell Biol. *33*, 429–443. https://doi.org/10.1128/MCB.00850-12.

Condie, B.G., Brivanlou, A.H., and Harland, R.M. (1990). Most of the homeobox-containing Xhox 36 transcripts in early xenopus embryos cannot encode a homeodomain protein. Mol. Cell Biol.

10, 3376–3385. https://doi.org/10.1128/mcb.10.7.3376-3385.1990.

Dadi, H., Jones, T.A., Merico, D., Sharfe, N., Ovadia, A., Schejter, Y., Reid, B., Sun, M., Vong, L., Atkinson, A., et al. (2018). Combined immunodeficiency and atopy caused by a dominant negative mutation in caspase activation and recruitment domain family member 11 (CARD11). J. Allergy Clin. Immunol. *141*, 1818–1830 e1812. https://doi.org/10.1016/j.jaci.2017.06.047.

David, L., Li, Y., Ma, J., Garner, E., Zhang, X., and Wu, H. (2018). Assembly mechanism of the CARMA1-BCL10-MALT1-TRAF6 signalosome. Proc. Natl. Acad. Sci. U S A *115*, 1499–1504. https://doi.org/10.1073/pnas.1721967115.

Dorjbal, B., Stinson, J.R., Ma, C.A., Weinreich, M.A., Miraghazadeh, B., Hartberger, J.M., Frey-Jakobs, S., Weidinger, S., Moebus, L., Franke, A., et al. (2019). Hypomorphic caspase activation and recruitment domain 11 (CARD11) mutations associated with diverse immunologic phenotypes with or without atopic disease. J. Allergy Clin. Immunol. *143*, 1482–1495. https://doi.org/10.1016/j.jaci.2018.08.013.

Duwel, M., Welteke, V., Oeckinghaus, A., Baens, M., Kloo, B., Ferch, U., Darnay, B.G., Ruland, J., Marynen, P., and Krappmann, D. (2009). A20 negatively regulates T cell receptor signaling to NF-kappaB by cleaving Malt1 ubiquitin chains. J. Immunol. *182*, 7718–7728. https://doi.org/10.4049/jimmunol.0803313.

Fang, H., Zhang, P., Huang, L.P., Zhao, Z., Pi, F., Montemagno, C., and Guo, P. (2014). Binomial distribution for quantification of protein subunits in biological nanoassemblies and functional nanomachines. Nanomedicine *10*, 1433–1440. https://doi.org/10.1016/j.nano.2014.03.005.

Gehring, T., Erdmann, T., Rahm, M., Grass, C., Flatley, A., O'Neill, T.J., Woods, S., Meininger, I., Karayel, O., Kutzner, K., et al. (2019). MALT1 phosphorylation controls activation of T lymphocytes and survival of ABC-DLBCL tumor cells. Cell Rep. *29*, 873–888 e810. https://doi.org/10.1016/j.celrep.2019.09.040.

Greil, J., Rausch, T., Giese, T., Bandapalli, O.R., Daniel, V., Bekeredjian-Ding, I., Stutz, A.M., Drees, C., Roth, S., Ruland, J., et al. (2013). Whole-exome sequencing links caspase recruitment domain 11 (CARD11) inactivation to severe combined immunodeficiency. J. Allergy Clin. Immunol. *131*, 1376–1383 e1373. https://doi.org/10.1016/j.jaci.2013.02.012.

Hamilton, K.S., Phong, B., Corey, C., Cheng, J., Gorentla, B., Zhong, X., Shiva, S., and Kane, L.P. (2014). T cell receptor-dependent activation of mTOR signaling in T cells is mediated by Carma1 and MALT1, but not Bcl10. Sci. Signal. *7*, ra55. https://doi.org/10.1126/scisignal.2005169.

Hara, H., Wada, T., Bakal, C., Kozieradzki, I., Suzuki, S., Suzuki, N., Nghiem, M., Griffiths, E.K., Krawczyk, C., Bauer, B., et al. (2003). The MAGUK family protein CARD11 is essential for lymphocyte activation. Immunity *18*, 763–775. https://doi.org/10.1016/s1074-7613(03)00148-1.

Hutcherson, S.M., Bedsaul, J.R., and Pomerantz, J.L. (2021). Pathway-specific defects in T, B, and NK cells and age-dependent development of high IgE in mice heterozygous for a CADINS-associated dominant negative CARD11 allele. J. Immunol. *207*, 1150–1164. https://doi.org/10.4049/jimmunol.2001233.

Izadi, N., Bauman, B.M., Dabbah, G., Thauland, T.J., Butte, M.J., Snow, A.L., and Church, J.A. (2021). CADINS in an adult with chronic sinusitis and atopic disease. J. Clin. Immunol. *41*, 256–258. https://doi.org/10.1007/s10875-020-00893-5.

Jattani, R.P., Tritapoe, J.M., and Pomerantz, J.L. (2016a). Cooperative control of caspase recruitment domain-containing protein 11 (CARD11) signaling by an unusual array of redundant repressive elements. J. Biol. Chem. *291*, 8324–8336. https://doi.org/10.1074/jbc.M115.683714.

Jattani, R.P., Tritapoe, J.M., and Pomerantz, J.L. (2016b). Intramolecular interactions and regulation of cofactor binding by the four repressive elements in the caspase recruitment domain-containing protein 11 (CARD11) inhibitory domain. J. Biol. Chem. *291*, 8338–8348. https://doi.org/10.1074/jbc.M116.717322.

Juilland, M., and Thome, M. (2018). Holding all the CARDs: how MALT1 controls CARMA/CARD-Dependent signaling. Front. Immunol. *9*, 1927. https://doi.org/10.3389/fimmu.2018.01927.

Jun, J.E., Wilson, L.E., Vinuesa, C.G., Lesage, S., Blery, M., Miosge, L.A., Cook, M.C., Kucharska, E.M., Hara, H., Penninger, J.M., et al. (2003). Identifying the MAGUK protein Carma-1 as a central regulator of humoral immune responses and atopy by genome-wide mouse mutagenesis. Immunity *18*, 751–762. https://doi.org/10.1016/s1074-7613(03)00141-9.

Lamason, R.L., Kupfer, A., and Pomerantz, J.L. (2010a). The dynamic distribution of CARD11 at the immunological synapse is regulated by the inhibitor kinesin GAKIN. Mol. Cell *40*, 798–809. https://doi.org/10.1016/j.molcel.2010.11.007.

Lamason, R.L., McCully, R.R., Lew, S.M., and Pomerantz, J.L. (2010b). Oncogenic CARD11 mutations induce hyperactive signaling by disrupting autoinhibition by the PKC-responsive inhibitory domain. Biochemistry *49*, 8240–8250. https://doi.org/10.1021/bi101052d.

Li, S., Yang, X., Shao, J., and Shen, Y. (2012). Structural insights into the assembly of CARMA1 and BCL10. PLoS One *7*, e42775. https://doi.org/10.1371/journal.pone.0042775.

Lork, M., Staal, J., and Beyaert, R. (2019). Ubiquitination and phosphorylation of the CARD11-BCL10-MALT1 signalosome in T cells. Cell. Immunol. *340*, 103877. https://doi.org/10.1016/j.cellimm.2018.11.001.

Lu, H.Y., Biggs, C.M., Blanchard-Rohner, G., Fung, S.Y., Sharma, M., and Turvey, S.E. (2019). Germline CBM-opathies: from immunodeficiency to atopy. J. Allergy Clin. Immunol. *143*, 1661–1673. https://doi.org/10.1016/j.jaci.2019.03.009.

Lu, H.Y., Sharma, M., Sharma, A.A., Lacson, A., Szpurko, A., Luider, J., Dharmani-Khan, P., Shameli, A., Bell, P.A., Guilcher, G.M.T., et al. (2021). Mechanistic understanding of the combined immunodeficiency in complete human CARD11 deficiency. J. Allergy Clin. Immunol. *148*, 1559–1574.e13. https://doi.org/10.1016/j.jaci.2021.04.006.

Ma, C.A., Stinson, J.R., Zhang, Y., Abbott, J.K., Weinreich, M.A., Hauk, P.J., Reynolds, P.R., Lyons, J.J., Nelson, C.G., Ruffo, E., et al. (2017). Germline hypomorphic CARD11 mutations in severe atopic disease. Nat. Genet. *49*, 1192–1201. https://doi.org/10.1038/ng.3898.

MacKinnon, R. (1991). Determination of the subunit stoichiometry of a voltage-activated potassium channel. Nature *350*, 232–235. https://doi.org/10.1038/350232a0.

Matsumoto, R., Wang, D., Blonska, M., Li, H., Kobayashi, M., Pappu, B., Chen, Y., and Lin, X. (2005). Phosphorylation of CARMA1 plays a critical role in T cell receptor-mediated NF-kappaB activation. Immunity *23*, 575–585. https://doi.org/10.1016/j.immuni.2005.10.007.

McCully, R.R., and Pomerantz, J.L. (2008). The protein kinase C-responsive inhibitory domain of CARD11 functions in NF-kappaB activation to regulate the association of multiple signaling cofactors that differentially depend on Bcl10 and MALT1 for association. Mol. Cell Biol. *28*, 5668–5686. https://doi.org/10.1128/MCB.00418-08.

Meininger, I., and Krappmann, D. (2016). Lymphocyte signaling and activation by the CARMA1-BCL10-MALT1 signalosome. Biol. Chem. *397*, 1315–1333. https://doi.org/10.1515/hsz-2016-0216.

Meitlis, I., Allenspach, E.J., Bauman, B.M., Phan, I.Q., Dabbah, G., Schmitt, E.G., Camp, N.D., Torgerson, T.R., Nickerson, D.A., Bamshad, M.J., et al. (2020). Multiplexed functional assessment of genetic variants in CARD11. Am. J. Hum. Genet. *107*, 1029–1043. https://doi.org/10.1016/j.ajhg.2020.10.015.

Nakaya, M., Xiao, Y., Zhou, X., Chang, J.H., Chang, M., Cheng, X., Blonska, M., Lin, X., and Sun, S.C. (2014). Inflammatory T cell responses rely on amino acid transporter ASCT2 facilitation of glutamine uptake and mTORC1 kinase activation. Immunity *40*, 692–705. https://doi.org/10.1016/j.immuni.2014.04.007.

Naviaux, R.K., Costanzi, E., Haas, M., and Verma, I.M. (1996). The pCL vector system: rapid production of helper-free, high-titer, recombinant retroviruses. J. Virol. *70*, 5701–5705. https://doi.org/10.1128/JVI.70.8.5701-5705.1996.

Notarangelo, L.D., Bacchetta, R., Casanova, J.L., and Su, H.C. (2020). Human inborn errors of immunity: an expanding universe. Sci. Immunol. *5*, eabb1662. https://doi.org/10.1126/sciimmunol.abb1662.

O'Neill, T.J., Seeholzer, T., Gewies, A., Gehring, T., Giesert, F., Hamp, I., Grass, C., Schmidt, H., Kriegsmann, K., Tofaute, M.J., et al. (2021). TRAF6 prevents fatal inflammation by homeostatic suppression of MALT1 protease. Sci. Immunol. *6*, eabh2095. https://doi.org/10.1126/sciimmunol.abh2095.

Oeckinghaus, A., Wegener, E., Welteke, V., Ferch, U., Arslan, S.C., Ruland, J., Scheidereit, C., and Krappmann, D. (2007). Malt1 ubiquitination triggers NF-kappaB signaling upon T-cell activation. EMBO J. *26*, 4634–4645. https://doi.org/10.1038/sj.emboj.7601897.

Pedersen, S.M., Chan, W., Jattani, R.P., Mackie d, S., and Pomerantz, J.L. (2016). Negative regulation of CARD11 signaling and lymphoma

cell survival by the E3 ubiquitin ligase RNF181. Mol. Cell Biol. *36*, 794–808. https://doi.org/10.1128/MCB.00876-15.

Pelzer, C., Cabalzar, K., Wolf, A., Gonzalez, M., Lenz, G., and Thome, M. (2013). The protease activity of the paracaspase MALT1 is controlled by monoubiquitination. Nat. Immunol. *14*, 337–345. https://doi.org/10.1038/ni.2540.

Pomerantz, J.L. (2021). Reconsidering phosphorylation in the control of inducible CARD11 scaffold activity during antigen receptor signaling. Adv. Biol. Regul. *79*, 100775. https://doi.org/10.1016/j.jbior.2020.100775.

Pomerantz, J.L., Denny, E.M., and Baltimore, D. (2002). CARD11 mediates factor-specific activation of NF-kappaB by the T cell receptor complex. EMBO J. *21*, 5184–5194. https://doi.org/10.1093/emboj/cdf505.

Qiao, Q., Yang, C., Zheng, C., Fontan, L., David, L., Yu, X., Bracken, C., Rosen, M., Melnick, A., Egelman, E.H., and Wu, H. (2013). Structural architecture of the CARMA1/Bcl10/MALT1 signalosome: nucleation-induced filamentous assembly. Mol. Cell *51*, 766–779. https://doi.org/10.1016/j.molcel.2013.08.032.

Schairer, R., Hall, G., Zhang, M., Cowan, R., Baravalle, R., Muskett, F.W., Coombs, P.J., Mpamhanga, C., Hale, L.R., Saxty, B., et al. (2020). Allosteric activation of MALT1 by its ubiquitin-binding Ig3 domain. Proc. Natl. Acad. Sci. U S A *117*, 3093–3102. https://doi.org/10.1073/pnas.1912681117.

Schlauderer, F., Seeholzer, T., Desfosses, A., Gehring, T., Strauss, M., Hopfner, K.P., Gutsche, I., Krappmann, D., and Lammens, K. (2018). Molecular architecture and regulation of BCL10-MALT1 filaments. Nat. Commun. *9*, 4041. https://doi.org/10.1038/s41467-018-06573-8.

Schneider, C.A., Rasband, W.S., and Eliceiri, K.W. (2012). NIH Image to ImageJ: 25 years of image analysis. Nat. Methods *9*, 671–675. https://doi.org/10.1038/nmeth.2089.

Seeholzer, T., Kurz, S., Schlauderer, F., Woods, S., Gehring, T., Widmann, S., Lammens, K., and Krappmann, D. (2018). BCL10-CARD11 fusion mimics an active CARD11 seed that triggers constitutive BCL10 oligomerization and lymphocyte activation. Front. Immunol. *9*, 2695. https://doi.org/10.3389/fimmu.2018.02695.

Shinohara, H., Maeda, S., Watarai, H., and Kurosaki, T. (2007). IkappaB kinase beta-induced phosphorylation of CARMA1 contributes to CARMA1 Bcl10 MALT1 complex formation in B cells. J. Exp. Med. *204*, 3285–3293. https://doi.org/10.1084/jem.20070379.

Snow, A.L., Xiao, W., Stinson, J.R., Lu, W., Chaigne-Delalande, B., Zheng, L., Pittaluga, S., Matthews, H.F., Schmitz, R., Jhavar, S., et al. (2012). Congenital B cell lymphocytosis explained by novel germline CARD11 mutations. J. Exp. Med. *209*, 2247–2261. https://doi.org/10.1084/jem.20120831.

Sommer, K., Guo, B., Pomerantz, J.L., Bandaranayake, A.D., Moreno-Garcia, M.E., Ovechkina, Y.L., and Rawlings, D.J. (2005). Phosphorylation of the CARMA1 linker controls NF-kappaB activation. Immunity *23*, 561–574. https://doi.org/10.1016/j.immuni.2005.09.014.

Stepensky, P., Keller, B., Buchta, M., Kienzler, A.K., Elpeleg, O., Somech, R., Cohen, S., Shachar, I., Miosge, L.A., Schlesier, M., et al. (2013). Deficiency of caspase recruitment domain family, member 11 (CARD11), causes profound combined immunodeficiency in human subjects. J. Allergy Clin. Immunol. *131*, 477–485 e471. https://doi.org/10.1016/j.jaci.2012.11.050.

Sun, L., Deng, L., Ea, C.K., Xia, Z.P., and Chen, Z.J. (2004). The TRAF6 ubiquitin ligase and TAK1 kinase mediate IKK activation by BCL10 and MALT1 in T lymphocytes. Mol. Cell *14*, 289–301. https://doi.org/10.1016/s1097-2765(04)00236-9.

Tangye, S.G., Al-Herz, W., Bousfiha, A., Chatila, T., Cunningham-Rundles, C., Etzioni, A., Franco, J.L., Holland, S.M., Klein, C., Morio, T., et al. (2020). Human inborn errors of immunity: 2019 update on the classification from the international union of immunological societies expert committee. J. Clin. Immunol. *40*, 24–64. https://doi.org/10.1007/s10875-019-00737-x.

Tanner, M.J., Hanel, W., Gaffen, S.L., and Lin, X. (2007). CARMA1 coiled-coil domain is involved in the oligomerization and subcellular localization of CARMA1 and is required for T cell receptor-induced NF-kappaB activation. J. Biol. Chem. *282*, 17141–17147. https://doi.org/10.1074/jbc.M700169200.

Thys, A., Douanne, T., and Bidere, N. (2018). Post-translational modifications of the CARMA1-BCL10-MALT1 complex in lymphocytes and activated B-cell like subtype of diffuse large B-cell lymphoma. Front. Oncol. *8*, 498. https://doi.org/10.3389/fonc.2018.00498.

Trottier, M., and Guo, P. (1997). Approaches to determine stoichiometry of viral assembly components. J. Virol. *71*, 487–494. https://doi.org/10.1128/JVI.71.1.487-494.1997.

Turvey, S.E., Durandy, A., Fischer, A., Fung, S.Y., Geha, R.S., Gewies, A., Giese, T., Greil, J., Keller, B., McKinnon, M.L., et al. (2014). The CARD11-BCL10-MALT1 (CBM) signalosome complex: stepping into the limelight of human primary immunodeficiency. J. Allergy Clin. Immunol. *134*, 276–284. https://doi.org/10.1016/j.jaci.2014.06.015.

Walter, D.M., Venancio, O.S., Buza, E.L., Tobias, J.W., Deshpande, C., Gudiel, A.A., Kim-Kiselak, C., Cicchini, M., Yates, T.J., and Feldser, D.M. (2017). Systematic in vivo inactivation of chromatin-regulating enzymes identifies Setd2 as a potent tumor suppressor in lung adenocarcinoma. Cancer Res. *77*, 1719–1729. https://doi.org/10.1158/0008-5472.CAN-16-2159.

Wang, Z., Hutcherson, S.M., Yang, C., Jattani, R.P., Tritapoe, J.M., Yang, Y.K., and Pomerantz, J.L. (2019). Coordinated regulation of scaffold opening and enzymatic activity during CARD11 signaling. J. Biol. Chem. *294*, 14648–14660. https://doi.org/10.1074/jbc.RA119.009551.

Yang, Y.K., Yang, C., Chan, W., Wang, Z., Deibel, K.E., and Pomerantz, J.L. (2016). Molecular determinants of scaffold-induced linear ubiquitinylation of B cell lymphoma/leukemia 10 (Bcl10) during T cell receptor and oncogenic caspase recruitment domain-containing protein 11 (CARD11) signaling. J. Biol. Chem. *291*, 25921–25936. https://doi.org/10.1074/jbc.M116.754028.

STAR★METHODS

KEY RESOURCES TABLE

REAGENT or RESOURCE	SOURCE	IDENTIFIER
Antibodies		
Rabbit monoclonal anti-Bcl10	Bethyl Laboratories	Cat#A303–579A; RRID:AB_11125535
Rabbit monoclonal anti-CARD11	Cell Signaling Technology	Cat#4435; RRID:AB_2070359; 1D12
Rabbit polyclonal anti-JNK2	Cell Signaling Technology	Cat#4672; RRID:AB_330915
Rabbit polyclonal anti-phospho-SAPK/JNK (Thr-183/Tyr-185)	Cell Signaling Technology	Cat #9251; RRID:AB_331659
Mouse monoclonal anti-linear ubiquitin	EMD Millipore	Cat#MABS451; LUB9
Mouse monoclonal anti-HOIP/RFN31	R&D Systems	Cat#MAB8039
Mouse monoclonal anti-c-Myc (referred to as anti-myc)	Santa Cruz	Cat#sc-40; RRID:AB_627268; 9E10
Mouse monoclonal anti-Bcl10	Santa Cruz	Cat#sc-5273; RRID:AB_626730; 331.3
Mouse monoclonal anti-MALT1	Santa Cruz	Cat#sc-46677; RRID:AB_627909; B-12
Mouse monoclonal anti-IKKα	Santa Cruz	Cat#sc-7606; RRID:AB_627784; B-8
Mouse monoclonal anti-cylindromatosis 1/CYLD	Santa Cruz	Cat#sc-74435; RRID:AB_1122022; E−10
Mouse monoclonal anti-RBCK1/HOIL-1	Santa Cruz	Cat#sc-393754; H-1
Rabbit polyclonal anti-FLAG	Sigma-Aldrich	Cat#F7425; RRID:AB_439687
Mouse monoclonal anti-FLAG	Sigma-Aldrich	Cat#F1804; RRID:AB_262044; M2
Sheep monoclonal anti-mouse IgG-horseradish peroxidase	Cytiva	Cat#NA931V; RRID:AB_772210
Donkey anti-rabbit IgG, whole Ab ECL, HRP conjugated	Cytiva	Cat#NA934V; RRID:AB_772206
Mouse monoclonal anti-CD3 human	BD Biosciences	Cat#555329; RRID:AB_395736
Mouse monoclonal anti-CD28 human	BD Biosciences	Cat#555725; RRID:AB_396068
Rat monoclonal anti-IgG1 mouse	BD Biosciences	Cat#553440; RRID:AB_394860
Bacterial and virus strains		
ElectroMAX DH10B cells	Invitrogen	Cat#18290015
Biological samples		
N/A	N/A	N/A
Chemicals, peptides, and recombinant proteins		
PfuUltra II Fusion HotStart DNA polymerase and 10x Reaction Buffer	Agilent	Cat#600672
nProtein A Sepharose 4 Fast Flow	Cytiva	Cat#17528001
Protein G Plus Sepharose	Cytiva	Cat#17061801
Blasticidin S HCl	Corning Inc.	Cat#30100RB
Pierce phosphatase inhibitor cocktail, 100x	Fisher	Cat#78420
Puromycin	Millipore Sigma	Cat#P8833
Protease inhibitor cocktail	Millipore Sigma	Cat#P8340
PMA	Millipore Sigma	Cat#P1585
Transit-LT1 Transfection Reagent	Mirus Bio	Cat#2306
Ionomycin calcium salt	Sigma-Aldrich	Cat#I06340
FLAG peptide 4 mg	Sigma-Aldrich	Cat#F53290
Polybrene	Sigma-Aldrich	Cat#H9268
Critical commercial assays		
IL-2 Human Uncoated ELISA kit	Invitrogen	Cat#88702588
β-gal Reporter Gene Assay, chemiluminescent	Roche	Cat#11758241001
Luciferase Assay System	Promega	Cat#E1501

(*Continued on next page*)

Continued

REAGENT or RESOURCE	SOURCE	IDENTIFIER
Deposited data		
N/A	N/A	N/A
Experimental models: Cell lines		
HEK293T cells	ATCC	RRID:CVCL_0063
Jurkat E6.1 cell line	ATCC	RRID:SCR_013869
CARD11-KO Jurkat T cells	Yang et al., 2016	N/A
CARD11-KO Jurkat E6.1-GFP	This paper	N/A
CARD11-KO Jurkat E6.1-Purocymin reconstituted with myc-WT-FLAGx2-Blasticidin	This paper	N/A
CARD11-KO Jurkat E6.1-Purocymin reconstituted with myc-N25Y CARD11-FLAGx2-Blasticidin	This paper	N/A
CARD11-KO Jurkat E6.1-Purocymin reconstituted with myc-E27K CARD11-FLAGx2-Blasticidin	This paper	N/A
CARD11-KO Jurkat E6.1-Purocymin reconstituted with myc-C28F CARD11-FLAGx2-Blasticidin	This paper	N/A
CARD11-KO Jurkat E6.1-Purocymin reconstituted with myc-R30W CARD11-FLAGx2-Blasticidin	This paper	N/A
CARD11-KO Jurkat E6.1-Purocymin reconstituted with myc-K41M CARD11-FLAGx2-Blasticidin	This paper	N/A
CARD11-KO Jurkat E6.1-Purocymin reconstituted with myc-Q55R CARD11-FLAGx2-Blasticidin	This paper	N/A
CARD11-KO Jurkat E6.1-Purocymin reconstituted with myc-E57D CARD11-2xFLAG-Blasticidin	This paper	N/A
CARD11-KO Jurkat E6.1-Purocymin reconstituted with myc-R72Q CARD11-FLAGx2-Blasticidin	This paper	N/A
CARD11-KO Jurkat E6.1-Purocymin reconstituted with myc-K83M CARD11-FLAGx2-Blasticidin	This paper	N/A
CARD11-KO Jurkat E6.1-Purocymin reconstituted with myc-H129D CARD11-FLAGx2-Blasticidin	This paper	N/A
Jurkat E6.1 reconstituted with myc-WT CARD11-FLAGx2-Blasticidin	This paper	N/A
Jurkat E6.1 reconstituted with myc-N25Y CARD11-FLAGx2-Blasticidin	This paper	N/A
Jurkat E6.1 reconstituted with myc-E27K CARD11-FLAGx2-Blasticidin	This paper	N/A
Jurkat E6.1 reconstituted with myc-C28F CARD11-FLAGx2-Blasticidin	This paper	N/A
Jurkat E6.1 reconstituted with myc-R30W CARD11-FLAGx2-Blasticidin	This paper	N/A
Jurkat E6.1 reconstituted with myc-K41M CARD11-FLAGx2-Blasticidin	This paper	N/A
Jurkat E6.1 reconstituted with myc-Q55R CARD11-FLAGx2-Blasticidin	This paper	N/A
Jurkat E6.1 reconstituted with myc-E57D CARD11-FLAGx2-Blasticidin	This paper	N/A
Jurkat E6.1 reconstituted with myc-R72Q CARD11-FLAGx2-Blasticidin	This paper	N/A
Jurkat E6.1 reconstituted with myc-K83M CARD11-FLAGx2-Blasticidin	This paper	N/A
Jurkat E6.1 reconstituted with myc-H129D CARD11-FLAGx2-Blasticidin	This paper	N/A
CARD11-KO Jurkat E6.1-GFP reconstituted with empty vector control-Blasticidin	This paper	N/A
CARD11-KO Jurkat E6.1-GFP reconstituted with myc-reQM CARD11-FLAGx2-Blasticidin	This paper	N/A
CARD11-KO Jurkat E6.1-GFP reconstituted with myc-E57D reQM CARD11-FLAGx2-Blasticidin	This paper	N/A

(*Continued on next page*)

Continued

REAGENT or RESOURCE	SOURCE	IDENTIFIER
CARD11-KO Jurkat E6.1-GFP reconstituted with myc-R72Q reQM CARD11-FLAGx2-Blasticidin	This paper	N/A
Jurkat E6.1 reconstituted with empty vector control-Blasticidin	This paper	N/A
Jurkat E6.1 reconstituted with myc-reQM CARD11-FLAGx2-Blasticidin	This paper	N/A
Jurkat E6.1 reconstituted with myc-E57D reQM CARD11-FLAGx2-Blasticidin	This paper	N/A
Jurkat E6.1 reconstituted with myc-R72Q reQM CARD11-FLAGx2-Blasticidin	This paper	N/A
Experimental models: Organisms/strains		
N/A	N/A	N/A
Oligonucleotides		
T7 promoter (for) for sequencing pcDNA3 vectors: 5′-TAATACGACTCACTATAGG-3′	JHU Sequencing Facility	N/A
Sp6 (rev) for sequencing pcDNA3 vectors: 5′-GATTTAGGTGACACTATAG-3′	JHU Sequencing Facility	N/A
N25Y (for) for site-directed mutagenesis: 5′-GGCCCTATGGGATTACGTGGAATGCAACCGG-3′	Integrated DNA Technologies	N/A
N25Y (rev) for site-directed mutagenesis: 5′-CCGGTTGCATTCCACGTAATCCCATAGGGCC-3′	Integrated DNA Technologies	N/A
E27K (for) for site-directed mutagenesis: 5′-CCTATGGGATAACGTGAAATGCAACCGGCACATGC-3′	Integrated DNA Technologies	N/A
E27K (rev) for site-directed mutagenesis: 5′-GCATGTGCCGGTTGCATTTCACGTTATCCCATAGG-3′	Integrated DNA Technologies	N/A
C28F (for) for site-directed mutagenesis: 5′-CAGCATGTGCCGGTTGAATTCCACGTTATCCC-3′	Integrated DNA Technologies	N/A
C28F (rev) for site-directed mutagenesis: 5′-GGGATAACGTGGAATTCAACCGGCACATGCTG-3′	Integrated DNA Technologies	N/A
R30W (for) for site-directed mutagenesis: 5′-CGTGGAATGCAACTGGCACATGCTGAGCCG-3′	Integrated DNA Technologies	N/A
R30W (rev) for site-directed mutagenesis: 5′-CGGCTCAGCATGTGCCAGTTGCATTCCACG-3′	Integrated DNA Technologies	N/A
K41M (for) for site-directed mutagenesis: 5′-CGTTACATCAACCCCGCCATGCTCACCCCCTACC-3′	Integrated DNA Technologies	N/A
K41M (rev) for site-directed mutagenesis: 5′-GGTAGGGGGTGAGCATGGCGGGGTTGATGTAACG-3′	Integrated DNA Technologies	N/A
R72Q (for) for site-directed mutagenesis: 5′-CAACAATCGGCCTGCTTGGTTGATCTTGGACGG-3′	Integrated DNA Technologies	N/A
R72Q (rev) for site-directed mutagenesis: 5′-CCGTCCAAGATCAACCAAGCAGGCCGATTGTTG-3′	Integrated DNA Technologies	N/A
pCLB3a-CARD11-mut (rev) for sequencing pCLB3a vectors: 5′-CCAAGTCCCGGCAACTGGAGG-3′	Integrated DNA Technologies	N/A
pCLB3a-H129D (for) for sequencing pCLB3a vector: 5′-GGATTACGTGGAATGCCACCG-3′	Integrated DNA Technologies	N/A
QMSfiI (for) for sequencing reQM vectors: 5′-CCGTCCAAGATCAACCGTGCAG-3′	Integrated DNA Technologies	N/A
QMSfiI (rev) for sequencing reQM vectors: 5′-CTCACGCAGTCCGGCCCTCTC-3′	Integrated DNA Technologies	N/A

(*Continued on next page*)

Continued

REAGENT or RESOURCE	SOURCE	IDENTIFIER
Recombinant DNA		
LentiCRISPRv2GFP (Plasmid #82416)	Walter et al., 2017	Addgene; Cat#82416
LentiCRISPRv2GFP-CARD11	This paper	N/A
pcDNA3	Invitrogen; McCully and Pomerantz, 2008	N/A
pCSK-LacZ	Gift from R. Harland; Condie et al., 1990	N/A
Igκ2-IFN-LUC	Pomerantz et al., 2002	N/A
psPax2 (Plasmid #12260)	Yang et al., 2016	Addgene#12259
pCL-Ampho	Gift from I.M. Verma; Naviaux et al., 1996	N/A
pCMV-VSV-G (Plasmid #8454)	Yang et al., 2016	N/A
FLAG-HOIP	Yang et al., 2016	N/A
FLAG-Bcl10	Gift from G. Nunez; McCully and Pomerantz, 2008	N/A
FLAG-MALT1	Chan et al., 2013	N/A
Untagged Bcl10	Chan et al., 2013	N/A
myc-WT CARD11 (previously referred to as pc-CARD11)	McCully and Pomerantz, 2008	N/A
myc-W23R CARD11	This paper	N/A
myc-N25Y CARD11	This paper	N/A
myc-E27K CARD11	This paper	N/A
myc-C28F CARD11	This paper	N/A
myc-N29I CARD11	This paper	N/A
myc-R30W CARD11	Dadi et al., 2018	N/A
myc-N38I CARD11	This paper	N/A
myc-A40T CARD11	This paper	N/A
myc-K41M CARD11	This paper	N/A
myc-T43I CARD11	This paper	N/A
myc-L46P CARD11	This paper	N/A
myc-E54G CARD11	This paper	N/A
myc-E54K CARD11	This paper	N/A
myc-Q55R CARD11	This paper	N/A
myc-D56N CARD11	This paper	N/A
myc-E57D CARD11	This paper	N/A
myc-L61H CARD11	This paper	N/A
myc-G74D CARD11	This paper	N/A
myc-K83M CARD11	This paper	N/A
myc-S94I CARD11	This paper	N/A
myc-L95Q CARD11	This paper	N/A
myc-Y103N CARD11	This paper	N/A
myc-R113L CARD11	This paper	N/A
myc-T117I CARD11	This paper	N/A
myc-V120L CARD11	This paper	N/A
myc-T128A CARD11	This paper	N/A
myc-H129D CARD11	This paper	N/A
myc-reQM CARD11 (previously referred to as re1 re2 re3 re4)	Jattani et al., 2016a	N/A

(*Continued on next page*)

Continued

REAGENT or RESOURCE	SOURCE	IDENTIFIER
myc-N25Y reQM CARD11	This paper	N/A
myc-E27K reQM CARD11	This paper	N/A
myc-C28F reQM CARD11	This paper	N/A
myc-R30W reQM CARD11	This paper	N/A
myc-K41M reQM CARD11	This paper	N/A
myc-Q55R reQM CARD11	This paper	N/A
myc-E57D reQM CARD11	This paper	N/A
myc-R72Q reQM CARD11	This paper	N/A
myc-K83M reQM CARD11	This paper	N/A
myc-H129D reQM CARD11	This paper	N/A
pCLB3a	Yang et al., 2016	N/A
pCLB3a-myc-WT CARD11-FLAGx2 previously referred to as FLAG-tagged CARD11	Wang et al., 2019	N/A
pCLB3a-myc-N25Y CARD11-FLAGx2	This paper	N/A
pCLB3a-myc-E27K CARD11-FLAGx2	This paper	N/A
pCLB3a-myc-C28F CARD11-FLAGx2	This paper	N/A
pCLB3a-myc-R30W CARD11-FLAGx2	This paper	N/A
pCLB3a-myc-K41M CARD11-FLAGx2	This paper	N/A
pCLB3a-myc-Q55R CARD11-FLAGx2	This paper	N/A
pCLB3a-myc-E57D CARD11-FLAGx2	This paper	N/A
pCLB3a-myc-R72Q CARD11-FLAGx2	This paper	N/A
pCLB3a-myc-K83M CARD11-FLAGx2	This paper	N/A
pCLB3a-myc-H129D CARD11-FLAGx2	This paper	N/A
pCLB3a-myc-reQM CARD11-FLAGx2 previously referred to as FLAG-tagged reQM CARD11	Wang et al., 2019	N/A
pCLB3a-myc-E57D reQM CARD11-FLAGx2	This paper	N/A
pCLB3a-myc-R72Q reQM CARD11-FLAGx2	This paper	N/A
Software and algorithms		
ImageJ v1.51j8	Schneider et al., 2012	https://imagej.nih.gov/ij/
GraphPad Prism 9.1.0	GraphPad Software Inc	https://www.graphpad.com/scientific-software/prism/
Serial Cloner 2.6.1	Serial Basics	http://serialbasics.free.fr/Serial_Cloner.html
PyMOL 2.3.4	PyMOL by Schrodinger	https://pymol.org/
AD/LD ANALYSIS SOFTWARE	Beckman Coulter	OEM#394145; https://www.partssource.com/parts/beckman-coulter/394145
Adobe Illustrator 2021	Adobe	https://www.adobe.com/products/illustrator.html
Microsoft 365 Excel	Microsoft Office	https://www.office.com/
Other		
Immunoprecipitation lysis buffer (IPLB)	McCully and Pomerantz, 2008	N/A
Denatured immunoprecipitation lysis buffer (DIPLB)	Yang et al., 2016	N/A

RESOURCE AVAILABILITY

Lead contact

Please direct all communication and requests for resources or reagents to the lead contact, Joel Pomerantz (joel.pomerantz@jhmi.edu).

Materials availability

Newly generated plasmids, primers, and genetically modified cell lines in this study are available from the lead contact upon request.

Data and code availability

- All data reported in this study will be available upon request by the lead contact.
- This study does not report original code.
- Any additional information required to reanalyze the data reported in this paper is available from the lead contact upon request.

EXPERIMENTAL MODEL AND SUBJECT DETAILS

Cell lines

HEK293T cells were obtained from the American Tissue Culture Collection (ATCC) and cultured in DMEM with 10% heat-inactivated FBS, 1× Penicillin and Streptomycin, and 0.4 mM L-Glutamine. Jurkat E6.1 T cells were purchased from ATCC and were cultured in RPMI with 0.4% β-mercaptoethanol, 10% heat-inactivated FBS, 1× Penicillin and Streptomycin, and 0.4 mM L-Glutamine (McCully and Pomerantz, 2008). CARD11 knockout (CARD11-KO) Jurkat T cells with puromycin resistance were generated previously through CRISPR/Cas9-mediated genome editing and were cultured with 0.5 μg/mL puromycin (Millipore Sigma, P8833) (Yang et al., 2016). CARD11-KO Jurkat T cells that were selected via GFP expression were generated in this study through CRISPR/Cas9-mediated genome editing. All cells stably reconstituted with CARD11 variants were generated through retroviral transduction and selection with 0.75–3 μg/mL blasticidin (Corning Inc., 30100RB). All cell lines were grown and maintained at 37°C in 5% CO_2.

METHODS DETAILS

Site-directed mutagenesis

Mutant CARD11 constructs in pcDNA3 (McCully and Pomerantz, 2008) or in the Moloney Murine Leukemia Virus-based retroviral vector, pCLB3a (Yang et al., 2016), containing the blasticidin resistance gene, were generated via standard cloning methods and site directed mutagenesis using the QuikChange Site-Directed Mutagenesis manufacturer's protocol. The following PCR set up was used: 50 ng in 5 μL of CARD11 vector template (10 ng/μL stock), 1 μL of a 10 μM stock each forward and reverse primer, 1 μL of a 10 mM stock of each dNTP as a dNTP solution, 5 μL of a 10× stock of PfuUltra II Fusion Buffer, 36.5 μL H_2O and 0.5 μL PfuUltra II Fusion HS DNA polymerase (Agilent, 600672) for 50 μL total per reaction. The PCR settings include 94°C for 4 min, followed by 16 cycles of 94°C for 30s, 55°C for 30s, and 72°C for 10 min, with final extension at 72°C for 15 min. Samples were kept at 4°C until further use. A total of 5 μL of the PCR product was digested overnight at 37°C with the DpnI restriction enzyme with 10x CutSmart and H_2O for a 20 μL reaction to remove the parental template DNA before transformation. A total of 1 μL of the digestion product was used to transform DH10B cells (Invitrogen, 18290015) via electroporation with the following settings: 1.6kV, 150 μsec, and 7 pulses. Standard molecular cloning techniques were used to isolate the plasmid and back clone the newly generated mutations into the parent template vector to ensure no additional mutations were present. Constructs were generated and sequence verified with the indicated primers in the key resources table. All recombinant DNA generated and used in this study is listed in the key resources table.

Determination of equivalent CARD11 protein expression in HEK293T cells

HEK293T cells were plated at a density of 5 × 10^5 cells in 2 mL per well in 6-well plates and after 22–24 h, the calcium phosphate method was used to transfect the cells with 200 ng of pCSK-LacZ (Condie et al., 1990), with or without 1500 ng of Igκ_2-IFN-LUC (Pomerantz et al., 2002), with or without the indicated amount of the pcDNA3 myc-CARD11 constructs, and the empty pcDNA3 vector to achieve 3000 ng of total DNA per condition. At 24 h post transfection, the media was replaced with 2 mL fresh complete DMEM and at 40–44 h post transfection, the cells were harvested in 400 μL 1× Reporter Lysis Buffer followed by incubation on ice for 10 min and centrifugation at 13,000 rpm for 10 min at 4°C. The chemiluminescent β-gal reporter gene assay (Roche, 11758241001) was performed using 2 μL of lysate according to the manufacturer's instructions using a Berthold Technologies TriStarLB 941 luminometer, integrating for 10 s after a 2 s delay. The measured β-gal activity was used to normalize for transfection efficiency and extract recovery and

the normalized lysates were resolved by SDS-PAGE, transferred to PVDF membranes, and analyzed by western blotting with the mouse anti-myc primary antibody (Santa Cruz, sc-40) and the sheep anti-mouse (Cytiva, NA931V) secondary antibody to determine relative expression. Western blots represent one of at least two replicate experiments.

Co-immunoprecipitations in HEK293T cells

HEK293T cells were plated at a density of 5 × 10^5 cells in 2 mL per well in 6-well plates and transfected 22–24 h later using the calcium phosphate method with either 200 ng of FLAG-Bcl10 (McCully and Pomerantz, 2008) or 100 ng of FLAG-HOIP (Yang et al., 2016), or 300 ng of untagged Bcl10 (Chan et al., 2013) and 500 ng of FLAG-MALT1 (Chan et al., 2013) with the indicated amount of the pcDNA3 myc-CARD11 constructs, and the empty pcDNA3 vector to reach 2000 ng of total DNA. Media was replaced with 2 mL fresh complete DMEM 24 h post transfection and cells were harvested 40–-41 h post transfection with 500 μL immunoprecipitation lysis buffer (IPLB) (McCully and Pomerantz, 2008) with protease inhibitor cocktail (Sigma, F8340). Lysed cells were incubated on ice for 10 min, cell debris was cleared by centrifugation at 13,000 rpm for 10 min at 4°C, and 30 μL lysate was saved at −80°C as the input for western blotting, while 450 μL of the lysate was rotated at 4°C with 1 μg rabbit anti-FLAG antibody (Sigma, F7425) for 4 h. A bed volume of 10 μL Protein G Plus Sepharose (Cytiva, 17061801) was added to the samples for an additional 2 h of rotation at 4°C. Four washes with IPLB were performed by centrifugation of samples at 0.5 rcf for 30 s at 4°C, followed by aspiration, washing with 1.3 mL IPLB and rotation at 4°C for 5 min each wash. Elution was performed twice using 100 μg/mL FLAG peptide (Sigma, F53290) and eluate was combined and resolved via SDS-PAGE and transferred to PVDF membranes for Western blotting with the indicated primary antibodies and following secondary antibodies, sheep anti-mouse and donkey anti-rabbit (Cytiva, NA934V). Western blots are representative of at least two replicate experiments.

Transient transfection and NF-κB luciferase reporter assay in Jurkat T cells

Wild-type, CARD11-KO, and stably reconstituted Jurkat T cells were transiently transfected for the NF-κB luciferase reporter assay in 6-well plates with 5 × 10^5 cells in 2 mL of RPMI using Transit-LT-1 Transfection Reagent (Mirus Bio, 2306) according to the manufacturer's instructions. Cells were transfected with 200 ng of pCSK-LacZ, 1500 ng of Igκ_2-IFN-LUC, with or without the indicated amount of the pcDNA3 myc-CARD11 construct, and the empty pcDNA3 vector to achieve 3000 ng of DNA per condition. At 40–41 h post transfection, cells were stimulated with 1 μg/mL each of anti-CD3 (BD Biosciences, 555329), anti-CD28 (BD Biosciences, 555725), and anti-IgG (BD Biosciences, 553440), for 4-5 h. The luciferase and β-gal signals were measured, and fold activation was determined as follows. Cells were lysed in 150 μL of 1× Reporter Lysis Buffer for 10 min on ice and debris was removed by 5 min of centrifugation at 13,000 rpm at 4°C. The chemiluminescent β-gal reporter gene assay was performed using 25 μL of lysate according to the manufacturer's instruction and the measured β-gal activity was used to normalize for transfection efficiency and extract recovery as described above. The luciferase assay system (Promega E1501) was used to assess NF-κB activation. The luciferase assay was performed using 50 μL cell lysate on the Berthold Technologies TriStarLB 941 luminometer, integrating for 10 s after a 2 s delay. Data represent the averages of three technical replicate samples with standard deviations (SD) from one of at least two replicate experiments or are from multiple replicate experiments that were averaged.

Generation and validation of GFP-expressing CARD11-KO Jurkat T cells

CARD11-KO Jurkat T cells were generated through CRISPR/Cas9-mediated genome editing and selected via GFP expression using the lentiCRISPRv2GFP vector (Walter et al., 2017) (Addgene plasmid ID#: 82416) that was engineered to express a guide RNA targeting CARD11 (5′-CAATGACCTTACACTGACGC-3′). The vectors were packaged into lentiviruses in HEK293T cells that were plated at 5 × 10^5 cells per well in a 6-well plate and transfected using the LT1 method described above with 663 ng Pax2 (Yang et al., 2016) (Addgene 12259, Plasmid #12260), 446 ng pCMV-VSVG (Yang et al., 2016) (Addgene, Plasmid #8454), and 891 ng of the lentiCRISPRv2GFP-CARD11 vector for a total of 2000 ng/well. At 22 h post transfection, the media was replaced with 2 mL fresh complete RPMI 1640 medium. At 44 h post transfection, the cell supernatants containing virus were harvested and cleared of cell debris by centrifugation at 1,400 rpm for 5 min and 900 μL of the cleared supernatant and 8 μg/mL polybrene (Sigma, H9268) was added to a T25 flask of 5 × 10^6 Jurkat T cells. At 24 h post infection, media was replaced with fresh complete RPMI and cells rested for 2 h at 37 °C before GFP analysis. Roughly, 50 percent GFP positivity was confirmed in the population of cells via flow cytometry (BD FACSCelesta) 26 h post infection. Single cell plating and selection of clonal

populations was performed by limiting dilution and verification of knockout was performed via Western blotting for CARD11 expression.

Stable reconstitution of wild-type and CARD11-KO Jurkat T cells with CARD11 variants

The pCLB3A Moloney Murine Leukemia Virus-based retroviral vectors containing wild-type or mutant CARD11 with an N-terminal myc-tag and two C-terminal FLAG tags, denoted pCLB3a-myc-CARD11-FLAGx2 (Wang et al., 2019), were used to stably reconstitute CARD11-KO and wild-type Jurkat T cells. These vectors express cDNAs from the viral LTR at levels that are subsaturating for signaling and that mimic endogenous levels of CARD11 expression (Chan et al., 2013; Jattani et al., 2016b; Lamason et al., 2010a; Pomerantz et al., 2002; Wang et al., 2019; Yang et al., 2016). To package retroviruses, HEK293T cells were plated at 5×10^5 cells per well in a 6-well plate and transfected using the LT-1 method as described above using 430 ng pCMV-VSVg, 430 ng pCL-Ampho (Naviaux et al., 1996), and 1140 ng of the pCLB3A retroviral vector for a total of 2000 ng/well. At 22 h post transfection, the media was replaced with 2 mL fresh complete RPMI 1640 medium. At 44 h post transfection, the cell supernatants containing virus were harvested and cleared of cell debris by centrifugation at 1,400 rpm for 5 min and 900 μL of the cleared supernatant was added to 5×10^6 CARD11-KO or wild-type Jurkat T cells. The following day the cells infected with pCLB3A retroviruses were cultured in blasticidin at 3 μg/mL or 0.75 μg/mL for the reconstituted CARD11-KO and wild-type Jurkat T cells, respectively, for at least 10 days prior to analysis. Cell clones of wild-type Jurkat T cells that were stably expressing myc-WT-CARD11-FLAGx2 or myc-mutant CARD11-FLAGx2 constructs were isolated by limiting dilution and variant expression was verified by Western blotting.

Endogenous co-immunoprecipitation in Jurkat T cells

Co-immunoprecipitations from Jurkat T cell lysates were performed using a total of 5–10 × 10^7 wild-type and CARD11-KO Jurkat T cells that were stably reconstituted with myc- and FLAG-tagged CARD11 variants. Cells were first rested via incubation for 30 min at 37°C in complete RPMI in 50 mL conical tubes. Cells were then either unstimulated or stimulated with 50 ng/mL PMA (Sigma, P1585) and 1 μM ionomycin (Sigma, I06340) in 10 mL total RPMI for the indicated time points at 37°C. Cells were harvested at the indicated time points by incubation on ice for 10 min, followed by centrifugation for 5 min at 1,400 rpm at room temperature, aspiration of media, and lysis on ice in 1.3 mL IPLB with protease inhibitor cocktail for 20 min followed by centrifugation at 4°C for 10 min. A total of 30 μL of each cell lysate was saved at −80°C as the input samples. The remaining lysates were rotated for 4 h at 4°C with either 4 μg rabbit anti-FLAG or 2 μg mouse anti-Bcl10 (Santa Cruz, sc-5273) for the endogenous immunoprecipitation assays. The samples were then incubated with nProtein A Sepharose (Cytiva, 17528001) at 20 μL bed volume overnight with rotation at 4°C and washed 5 times for 10 min with rotation at 4°C as described above. On the last wash following centrifugation and aspiration, 50 μL of SDS loading buffer was added and the samples were spun via centrifugation for 10 s at 13,000 rpm at 4°C followed by heat treatment with the input samples at 95°C for 10 min. Next, centrifugation of the IP samples was performed for 10 s at 13,000 rpm at room temperature to pellet the beads and 45 μL of the input and IP samples in SDS loading buffer were resolved by SDS-PAGE and transferred to PVDF membranes, and Western blotting was performed with the indicated antibodies. Western blots are representative of one of at least two replicates of each experiment.

Denatured endogenous co-immunoprecipitation in Jurkat T cells

The denatured endogenous co-immunoprecipitation was performed with a total of 5×10^7–10×10^7 Jurkat T cells that were stably reconstituted with myc-CARD11-FLAGx2 variants. Cells were first rested via incubation for 30 min at 37°C in complete RPMI in 50 mL conical tubes. Next, cells were resuspended in 10 mL complete RPMI with or without 50 ng/mL PMA and 1 μM ionomycin at 37°C. At the indicated time points, cells were collected by incubation on ice for 10 min, followed by centrifugation for 5 min at 1,400 rpm at room temperature. Media was aspirated and cells were lysed on ice in 1.3 mL denatured immunoprecipitation lysis buffer (DIPLB) (Yang et al., 2016) with a protease inhibitor cocktail for 20 min followed by centrifugation at 4°C for 10 min to clear cell debris. SDS was added to the cleared lysates for a final concentration of 1% SDS and samples were heat treated for 5 min at 95°C. For the input sample, 30 μL of lysate was saved and stored at −80°C. The remaining sample was further diluted to 0.1% SDS by adding 10 mL of DIPLB and 10 μg of rabbit anti-Bcl10 antibody (Bethyl Laboratories, A303–579A) and the samples incubated with rotation at 4 °C for 4 h. The samples were then incubated with nProtein A Sepharose at 30 μL bed volume overnight with rotation at 4°C, washed 5 times for 10 min with rotation at 4 °C, and harvested and analyzed

as described above for the endogenous co-IP assay. Data represent one of at least two replicate experiments.

Determination of MALT1 protease and JNK activation

MALT1 protease and JNK activation were assessed as follows: 1-2 × 10^6 Jurkat T cells were incubated in 500 μL RPMI at 37°C for 30 min in 1.5 mL microcentrifuge tubes, and then unstimulated or stimulated with 1 μg/mL each of anti-CD3, anti-CD28, and anti-IgG in RPMI at 37°C for the time points indicated. Cells were harvested by incubation on ice for 10 min, followed by centrifugation at 4°C for 5 min at 1,400 rpm. Supernatant was aspirated and cells were lysed in 60-120 μL IPLB with Pierce phosphatase inhibitor cocktail (Fisher, 78420) and protease inhibitor cocktail and lysates incubated on ice for 10 min. Debris was cleared by centrifugation at 13,000 rpm for 10 min at 4°C and 30 μL of lysate with 15 μL 3× SDS buffer per sample was resolved via SDS-PAGE and transferred to PVDF membranes, and western blotting was performed using the indicated antibodies to assess MALT1 protease and JNK activation. Data are representative of one of at least two replicate experiments.

IL-2 ELISA

IL-2 production by Jurkat T cell lines was measured using the IL-2 Human Uncoated ELISA kit (Invitrogen, 88702588). A total of 5 × 10^5 cells were plated in triplicate in a 96-well flat bottom plate in a volume of 200 μL of complete RPMI or were stimulated with 5 μg/μL of anti-CD3, anti-CD28, and anti-IgG in 200 μL of complete RPMI for 24 h at 37°C. At 24 h, samples were collected in 1.5 mL microcentrifuge tubes followed by centrifugation at 1,400 rpm for 5 min to pellet cells. Cell supernatant was transferred to a new tube and frozen at −80°C or was used immediately for the IL-2 Human Uncoated ELISA according to the manufacturer's instructions. ELISA plates were analyzed on the Beckman Coulter AD340 using AD LD Analysis Software at a wavelength of 450 nm with the reference read at 570 nm. Data represent the mean IL-2 production in pg/mL with SD for one of at least two replicate experiments consisting of three replicates for each cell line (Figures 3H and 7H) or are the average of biological replicate experiments (Figure 4E).

QUANTIFICATION AND STATISTICAL ANALYSIS

Quantification of western blots

The relative protein levels were quantified using ImageJ (Schneider et al., 2012) as a ratio of the protein band relative to the specified loading control with the background for both subtracted from each band quantification. The relative protein values are the representative quantification from one of at least two replicate experiments and are included in Table 2 and figure legends.

Statistical analysis

All statistical analyses were conducted using GraphPad Prism 9.1.0. Statistics were calculated for the Jurkat T cell luciferase reporter assays and IL-2 ELISA assays using the two-tailed unpaired Student's *t* test to determine whether NF-κB activation and IL-2 production by each CARD11 LOF mutant was statistically significant from the activity of wild-type CARD11. The variance (SD) was comparable but not equal among wild-type and variant groups and therefore the t test was conducted with Welch's correction. The p values are included in corresponding figure legends.